Louisiana State University
LSU Digital Commons

LSU Doctoral Dissertations | Graduate School

7-2-2019

Observations of Lightning Produced Gamma-ray Flashes with TETRA-II

Donald John Pleshinger
Louisiana State University and Agricultural and Mechanical College

Follow this and additional works at: https://digitalcommons.lsu.edu/gradschool_dissertations

Recommended Citation

Pleshinger, Donald John, "Observations of Lightning Produced Gamma-ray Flashes with TETRA-II" (2019). *LSU Doctoral Dissertations*. 5005.
https://digitalcommons.lsu.edu/gradschool_dissertations/5005

This Dissertation is brought to you for free and open access by the Graduate School at LSU Digital Commons. It has been accepted for inclusion in LSU Doctoral Dissertations by an authorized graduate school editor of LSU Digital Commons. For more information, please contactgradetd@lsu.edu.

OBSERVATIONS OF LIGHTNING PRODUCED GAMMA-RAY FLASHES WITH TETRA-II

A Dissertation

Submitted to the Graduate Faculty of the
Louisiana State University and
Agricultural and Mechanical College
in partial fulfillment of the
requirements for the degree of
Doctor of Philosophy

in

The Department of Physics and Astronomy

by
Donald John Pleshinger
B.S., Ohio Northern University, 2013
August 2019

To me, nice job DJ

Acknowledgments

First and foremost, I thank my parents, John and Christine Pleshinger, who have supported and encouraged me throughout my studies. Thanks also to my sisters, Emily Cox and Kellie Pleshinger, and my brother, Matthew Pleshinger, for their support during this time.

I would like to thank the numerous staff members in the physics department, including Doug Granger, Brad Ellison, Doug Smith, and Michael Stewart for their significant help and discussions on the equipment and software with this work. I also thank postdocs Ching-Cheng Hsu and Samer Alnussirat, fellow graduate student and now PhD Nick Cannady, and the many undergraduate student workers who have spent time on this experiment. A special thanks to undergraduate Jonah Hoffman for putting up with me the past three years and for travelling on numerous occasions with me to fix broken equipment.

I would like to gratefully acknowledge funding from NSF (Office of Atmospheric and Geospace Sciences), NASA EPSCoR, the Louisiana Board of Regents, and Louisiana Space Consortium for the development and operation of TETRA-II, and the very helpful support of Milton Riutort and Edgar del Toro at the University of Puerto Rico-Utuado and Franklin Hurley and Javiar Arias at CENAMEP in Panama. Lightning data were provided by Vaisala and WWLLN.

Finally, I would like to thank my Ph.D. committee for providing comments and suggestions. I would like to thank Dr. Michael Cherry for giving me the opportunity to work in his lab and to learn from him and his experiences in the scientific community.

Table of Contents

List of Tables

List of Figures

Abstract

Terrestrial gamma-ray flashes (TGFs) are sub-millisecond duration intense bursts of gamma-rays discovered to be correlated with thunderstorms. These events, radiation associated with lightning leaders, and longer duration increases in rate have been observed both by satellites and detectors on the ground. The TGF and Energetic Thunderstorm Rooftop Array II (TETRA-II) experiment is a ground-based array of bismuth-germanate (BGO) scintillators deployed in Baton Rouge, Louisiana; Utuado, Puerto Rico; and Panama City, Panama to detect these thunderstorm-related events. After 3 years of operation, 23 gamma-ray bursts have been detected with an average duration of 970 μs with on average 70 photons detected in the 200 keV - 8 MeV energy range. Of the 23 events, 20 have a radio signal observed within 1.3 ms of the beginning of the event, indicating that these events are produced by the final stages of the lightning step leader process that occurs before the radio emission. The TETRA-II equipment and design, details on the short duration bursts, and a search for longer duration events are presented.

Chapter 1. Introduction

The main purpose of this dissertation is to study Terrestrial Gamma-ray Flashes (TGFs) and bursts of energetic radiation emitted during thunderstorms in association with lightning using the TGF and Energetic Thunderstorm Rooftop Array II (TETRA-II) equipment. Lightning provides one of the most powerful natural accelerators available on Earth for the production of high energy particles. Satellite instruments have detected gamma ray bursts at energies up to tens of MeV as a result of this acceleration. Initially, these TGFs were detected by the Burst and Transient Source Experiment (BATSE) on-board the Compton Gamma Ray Observatory in 1994 as extremely intense bursts on the order of hundreds of microseconds to a few milliseconds in duration (Fishman et al., 1994). Later observations have shown that these events are associated mainly with positive polarity intracloud (IC) lightning (lightning that originates in the positive charge region of a thundercloud and travels to a negatively charged region of a thundercloud) that generates the upward trajectory of electrons and photons, and are correlated with regions of intense lightning, typically 10 - 15 km above the ground (Rakov et al., 2003).

Since their discovery by satellites, TGFs and other thunderstorm-associated bursts of radiation have also been observed from the ground (Dwyer et al., 2004a; Mallick et al., 2012; Ringuette et al., 2013; Tran et al., 2015; Enoto et al., 2017). TETRA-I was operational from 2010 - 2014 and detected ∼30 TGFs originating from downward directed negative polarity cloud-to-ground (CG) lightning (lightning that originates in the negative charge region of a thundercloud and travels to the ground) (Ringuette et al., 2013). By using scintillators with a higher energy range, faster electronics, and additional locations with high lightning activity, TETRA-II is an improved array to more efficiently detect ground level gamma-ray flashes produced by lightning strikes. Searching for events from the ground places the detectors significantly closer to the source of the events, allowing for the detection of weaker events as well as better correlations with storm structures and lightning activity.

Further results in these areas will also allow for a better understanding of the production mechanisms for thunderstorm-associated gamma-ray bursts.

Presented here are the detection by the upgraded TGF and Energetic Thunderstorm Rooftop Array (TETRA-II) of 23 short bursts of photons at ground level simultaneously with Radio Frequency (RF) emission. In Chapter 2 the scientific background and motivation for this ground-based array are introduced. Chapter 3 describes the TETRA-II equipment used for observing the radiation bursts. Chapter 4 details the TETRA-II submillisecond duration gamma-ray observations, together with the correlations with various lightning detection networks. A search of the data for longer duration events is discussed in Chapter 5. Conclusions are presented in Chapter 6. Electronics and power schematics used for the TETRA-II equipment are included in Appendix A, and a detailed description of the processing of the raw data is given in Appendix B.

Chapter 2. Motivation

2.1 Previous Observations

Lightning provides one of the most powerful natural high-energy charged particle accelerator available on Earth. Satellite instruments have detected Terrestrial Gamma-ray Flashes (TGFs) - intense sub-millisecond bursts of bremsstrahlung photons at energies in excess of tens of MeV emitted by electrons and positrons accelerated by the electric fields associated with thunderstorms. TGFs were initially detected by the Burst and Transient Source Experiment (BATSE) on board the Compton Gamma-Ray Observatory (Fishman et al., 1994). Figure 2.1 shows a sample of short millisecond duration intense bursts that were observed by the sodium-iodide (NaI) scintillators on board. These unique observations were then correlated with areas of thunderstorm activity on the Earth, not cosmic-ray events from extra-terrestrial sources.

Following the BATSE results, the Reuven Ramaty High Energy Solar Spectroscopic Imager (RHESSI), which began observing TGFs upon its deployment in 2002, published a map of over 800 events shown in Figure 2.2 (Smith et al., 2003; Grefenstette et al., 2009). This map shows the highest density of events is located in 3 regions of high thunderstorm activity, mostly near coastal regions: central America, western Africa, and southeast Asia. In addition to BATSE and RHESSI, TGFs have been observed and cataloged from space experiments BeppoSAX (Ursi et al., 2017) and RELEC (Panasyuk et al., 2016), and are currently being observed by the Gamma-ray Burst Monitor (GBM) on board the Fermi telescope (Roberts et al., 2018), the Large Area Telescope (LAT) also on Fermi (Grove et al., 2012), the Mini-Calorimeter (MCAL) on the AGILE satellite (Marisaldi et al., 2010), and most recently by the Atmosphere-Space Interactions Monitor (ASIM) on the International Space Station (ISS) (Østgaard et al., 2018).

Correlations between GBM TGFs and the World Wide Lightning Location Network (WWLLN) lightning sferic data (the radio signal emitted from the discharge of the return stroke) have been performed with an association rate of $\sim$30% (Connaughton et al., 2010).

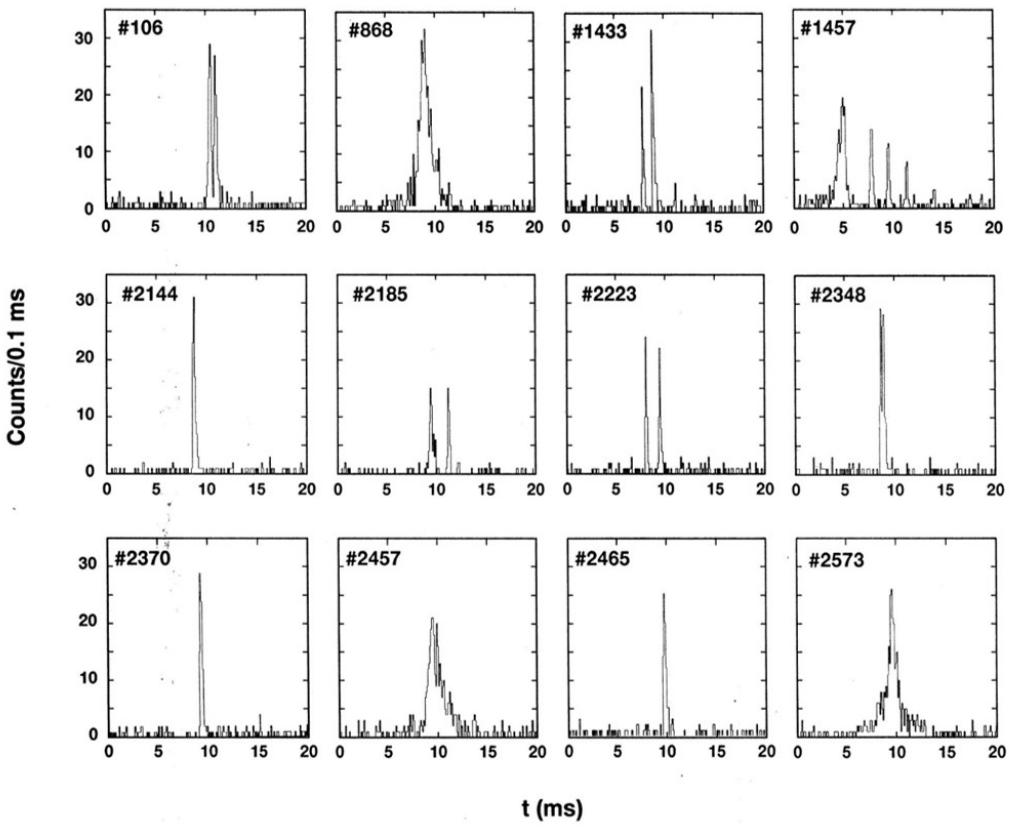

Figure 2.1. Time series binned in 100 μs bins of the initial TGF events observed by BATSE (Fishman et al., 1994).

These observations, associated mainly with positive polarity IC lightning that produces upward-moving charge, have been correlated with regions of intense lightning and source regions at the altitudes of thunderstorm tops, typically 10-15 km above ground level. In the atmosphere, a single event has been seen at aircraft altitude by the Airborne Detector for Energetic Lightning Emissions (ADELE) (Smith et al., 2011), while lightning-associated events have been reported at ground level by different experiments (Dwyer et al., 2004a; Ringuette et al., 2013; Tran et al., 2015; Dwyer et al., 2012; Enoto et al., 2017) along with the observation of radiation associated with lightning leaders (Moore et al., 2001; Dwyer et al., 2004b; Mallick et al., 2012). Related events have been detected by high-energy cosmic-ray detectors (Chilingarian et al., 2010; Abbasi et al., 2018).

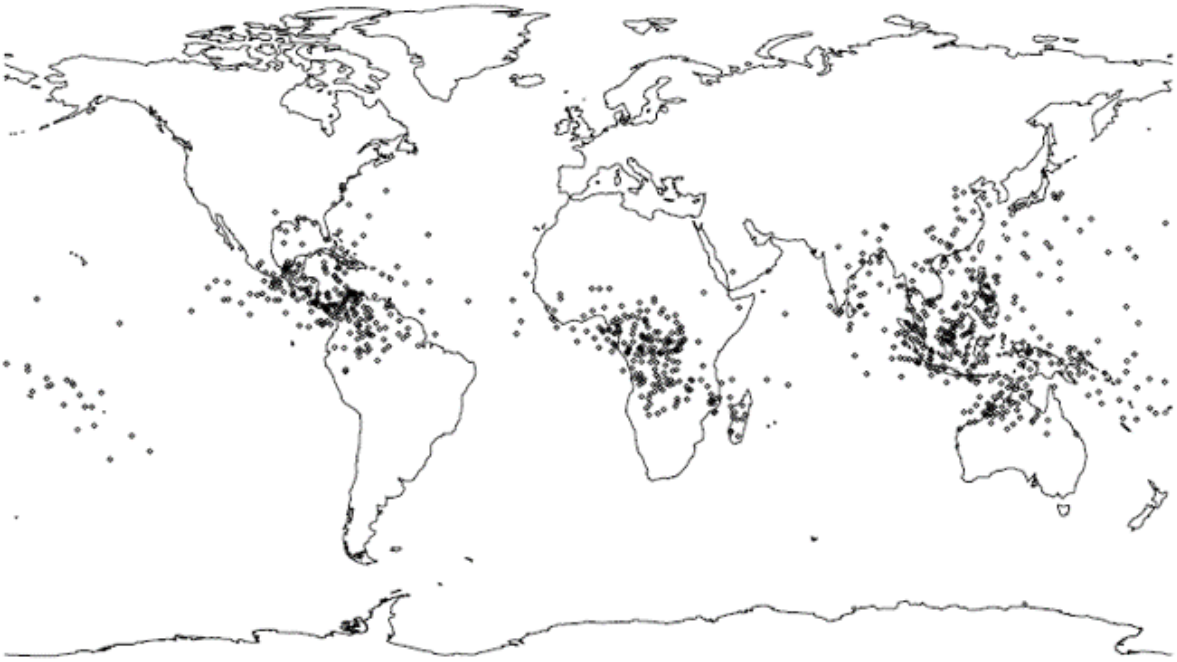

Figure 2.2. Map of over 800 TGFs observed by RHESSI since its launch in 2002 (Grefenstette et al., 2009)

An initial TETRA-I experiment was conducted at Louisiana State University (LSU) to search for TGFs and thunderstorm related bursts from the ground (Ringuette et al., 2013). There are many benefits to studying TGF and thunderstorm radiation from ground level where one is less than 5 km from the storms as opposed to using satellites hundreds of km away. As satellites have detected more and more TGFs and their properties have become better understood, their thresholds have decreased and triggering has improved. By moving detectors significantly closer to the source, it increases the possibility of observing weaker events that would not travel the much larger distances to satellites. Also, to better understand the production mechanisms of these events, the ability to correlate bursts with individual lightning strikes or storm cells is invaluable.

In 2011 TETRA-I had four separate boxes each containing three $0.635 \times 20.3 \times 20.3$ cm^3 NaI scintillators deployed on rooftops around the LSU campus in Baton Rouge, spaced out by $\sim$500 m. During its 4 years of operation, $\sim$30 millisecond-scale bursts were observed

in association with radio signals from negative polarity lightning strikes. Figure 2.3 shows an example of an event detected. The top row shows the sum of the photons in the 3 NaI detectors in a single box, with the following three rows showing the individual scintillators. All three observe a collection of hits at the same time, which when summed show an event that clearly stands out from the background. The bottom panel shows 1 Photomultiplier Tube (PMT) that was connected to the entire electronics system, but did not view an NaI. This was used as a check to monitor for any electronic noise during the time of events. The use of NaI scintillators put a limit on the observable energy range of events at $\sim$2 MeV, which is much lower than the tens of MeVs associated with satellite observed TGFs. Further details about the design and results of TETRA-I can be found in Ringuette et al. (2013).

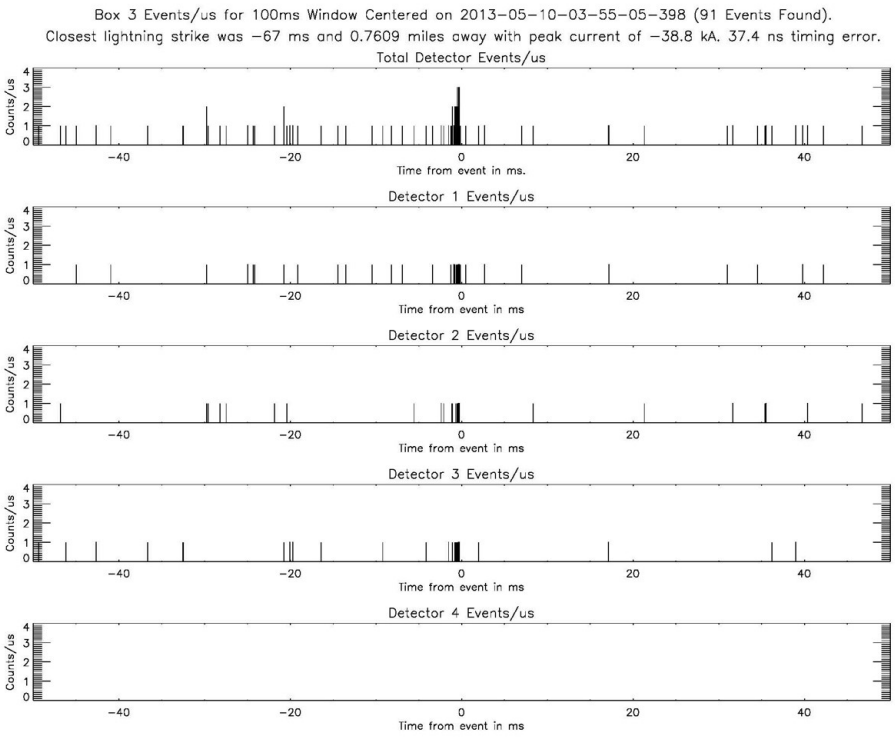

Figure 2.3. Sample of an event observed by TETRA-I. Top panel shows the sum of the 3 NaI scintillators. The middle 3 panels are the individual NaI time series. The bottom panel shows a PMT not viewing a scintillator to monitor for noise.

TETRA-I also compared the times of its observed events with local radar data. Figure 2.4 shows radar images in 5 minute intervals during a storm on 22 June 2013 that produced two bursts observed by TETRA-I. Here the two gamma-ray flashes separated by 20 minutes can be seen in the bottom left and top right panels. At both of these times, the cloud top and precipitation heights had increased up from ∼30,000 ft to ∼40,000 ft. This pattern of events occurring during this updraft phase of the thunderstorm was observed for many of the TETRA-I reported TGFs; however, with the limitation of 5 minute interval radar images this analysis is seen only as proof that further weather and storm cell correlation studies can be done with ground-based detections. This collection of bursts of photons during thunderstorms in association with lightning strikes and radar images gave the motivation to construct the larger, more sensitive array, TETRA-II.

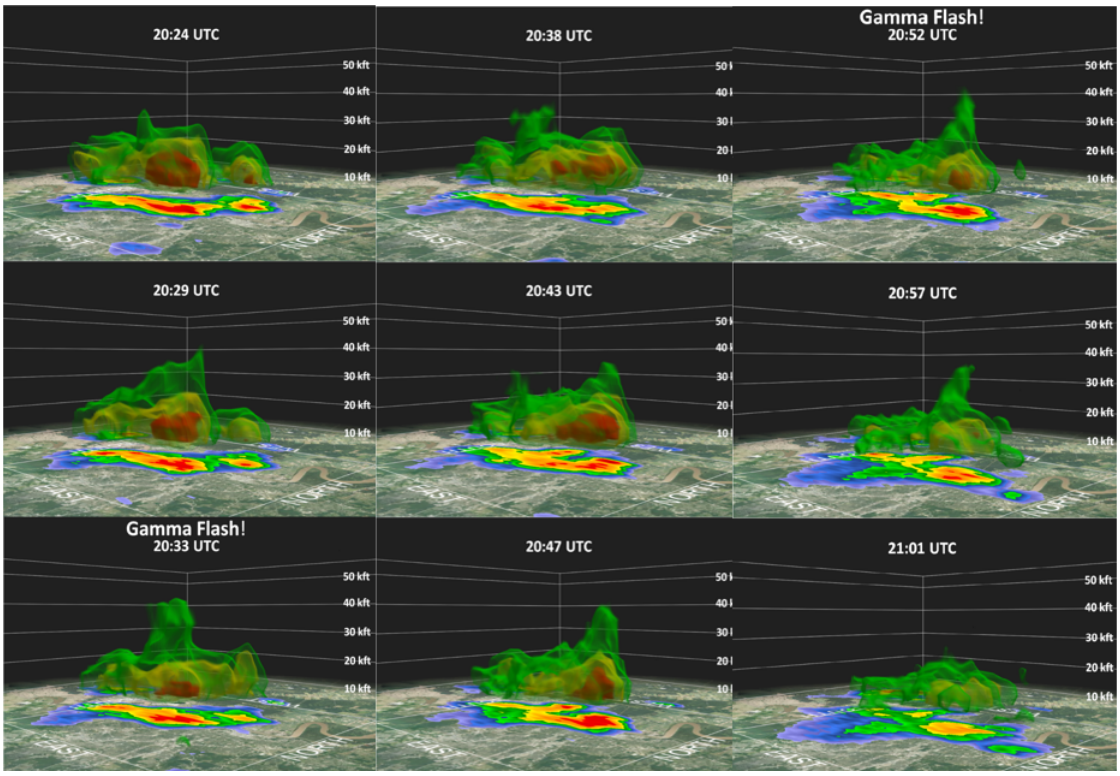

Figure 2.4. Radar data centered on TETRA-I equipment at LSU in 5 minute intervals, going top to bottom then left to right. An increase in precipitation height or the collapse of this updraft is observed at the time of the two observed bursts during a storm on 22 June 2013 (Ringuette et al., 2013).

TETRA-II is an improved array to observe and collect data from downward directed gamma-ray bursts and further study their correlation with lightning strikes and thunderstorm cells. With the continued success of satellite observations with significant location uncertainty, and the new results observing downward directed events, these observations will provide more information to further the understanding of TGFs and lightning produced gamma-ray emissions. Presented here is the first collection of lightning-associated gamma-ray bursts observed by the TETRA-II experiment.

2.2 Production Mechanisms

Electron acceleration in the atmosphere is affected by both the strength of the electric field and the collisional and radiative effects encountered by the particle. In order to create a TGF, an intense shower of high energy electrons must be produced by a sufficiently strong electric field, so that the energy gains outweigh the energy losses in the atmosphere. Figure 2.5 shows a solid curve depicting the energy loss of an electron travelling in the atmosphere due to collisions and a dashed line for losses due to radiative processes. The energy added by the electric field is shown by the horizontal line labeled eE, and it can be seen that once above a threshold energy, ϵ_{th}, the electrons will gain energy faster than they lose it. Within a thunderstorm the field is $\sim 2.84 \times 10^5$ n V / m, where n is the ratio of the density of air compared to the density of air at standard temperature and pressure (STP) (Dwyer, 2008). The more dense the air, the higher the likelihood of energy loss, so a higher field is required at the same electron energy. The accelerated electrons can knock off secondary electrons by electron impact ionization, which can themselves be accelerated, producing avalanches of electrons. These electrons will produce photons via bremsstrahlung, and the photons may generate electron-positron pairs, which can be accelerated further by the electric field.

Bremsstrahlung photons are the result of a charged particle being decelerated due to collisions with air molecules and are the photons observed as TGFs. To continue this runaway process, there are 3 interaction processes that the photons can undergo to produce further electrons and positrons, depicted in Figure 2.6 with data taken from the National In-

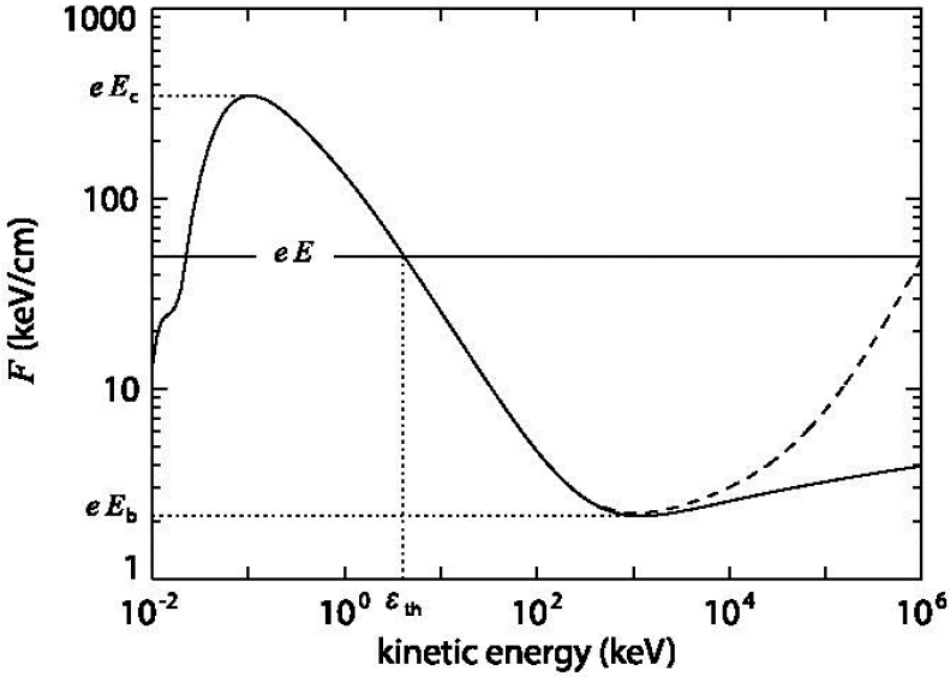

Figure 2.5. Curve shows the energy loss dE/dx of an electron due to interactions. The horizontal line is the energy gain from the electric field. Once the electron is above the threshold value ϵ_{th} the particle will gain energy faster than it loses energy and will run-away. The dashed line represents the energy losses due to radiative processes, and is seen to be more dominant than the interactions above the break-even field E_b
(Dwyer, 2012)

stitute of Standards and Technology (NIST) XCOM photon cross sections database (NIST XCOM, 2018). At low photon energies, typically less than 100 keV, photoionization is the dominant process. Here, the incoming photon hits a target material or atom and is completely absorbed via the photoelectric effect, emitting an electron(s) in the process. In the 100 keV up to 10s of MeV range Compton scattering is most common. This process involves a photon scattering off of an electron or other charged particle giving a portion of its energy to the particle. The third process, pair production, requires a photon of energy at least $2 \times m_o c^2$ (1.022 MeV), and produces an electron - positron pair by the annihilation of the photon.

Each of these processes can produce additional electrons to continue the process, with the most common being electron - electron (Møller) scattering. With a relativistic seed electron accelerated by the large-scale ambient electric field between opposite charge layers in a thundercloud, the Relativistic Runaway Electron Avalanche (RREA) process can take place (Dwyer, 2003). The multiplication of electrons in RREA has been studied in great depth in association with TGFs as the main process producing the fluxes of photons and spectra observed. RHESSI TGF spectra were compared with Monte Carlo simulations of the RREA process and were seen to be in agreement with a characteristic energy of the runaway electrons of ∼7 MeV (Dwyer et al., 2005).

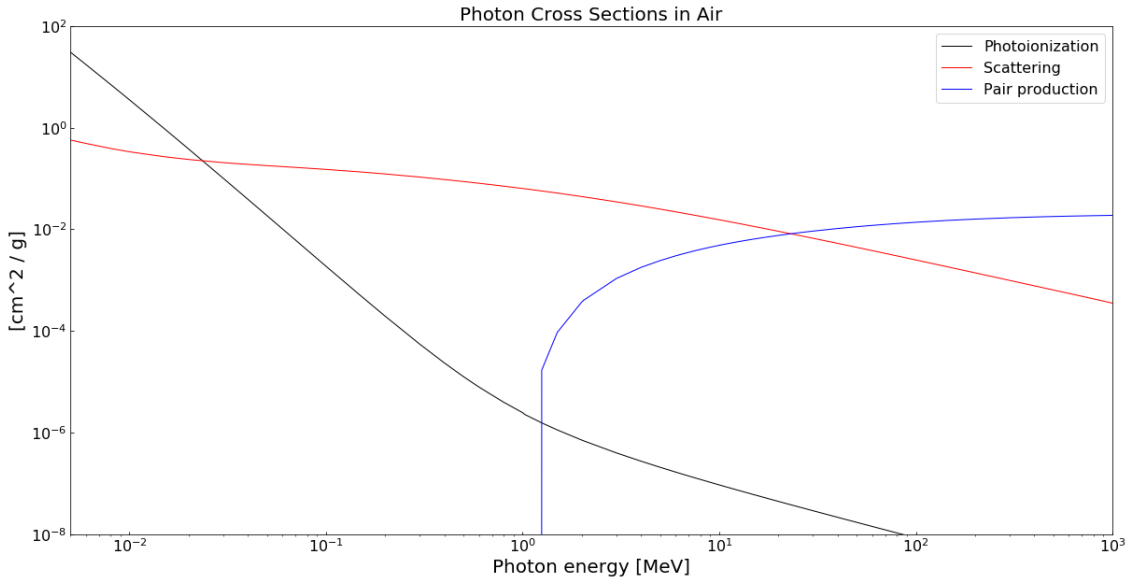

Figure 2.6. Cross sections of photons showing the dominant interaction process in air.

Two main mechanisms are discussed as the source of TGFs. The first process involves a feedback mechanism to create additional avalanches (Gurevich et al., 1992; Roussel-Dupre et al., 1996; Dwyer, 2003, 2012). In this case an initial highly energetic seed electron can create a shower of electrons and bremsstrahlung photons; however, modelling has proved this to be insufficient to produce the photon flux observed (Dwyer, 2008). With the production of positrons from pair production along with back-scattered photons both moving in the opposite direction to the electrons, new seed electrons can be formed creating

additional avalanches (Dwyer, 2012). This process is shown in the left of Figure 2.7. The combination of this Relativistic Feedback process with RREA can produce spectra and photon fluxes similar to those seen in satellite-detected TGFs. In this scenario, TGFs would be emitted independent of lightning activity and rely solely on the ambient electric field within a thunderstorm.

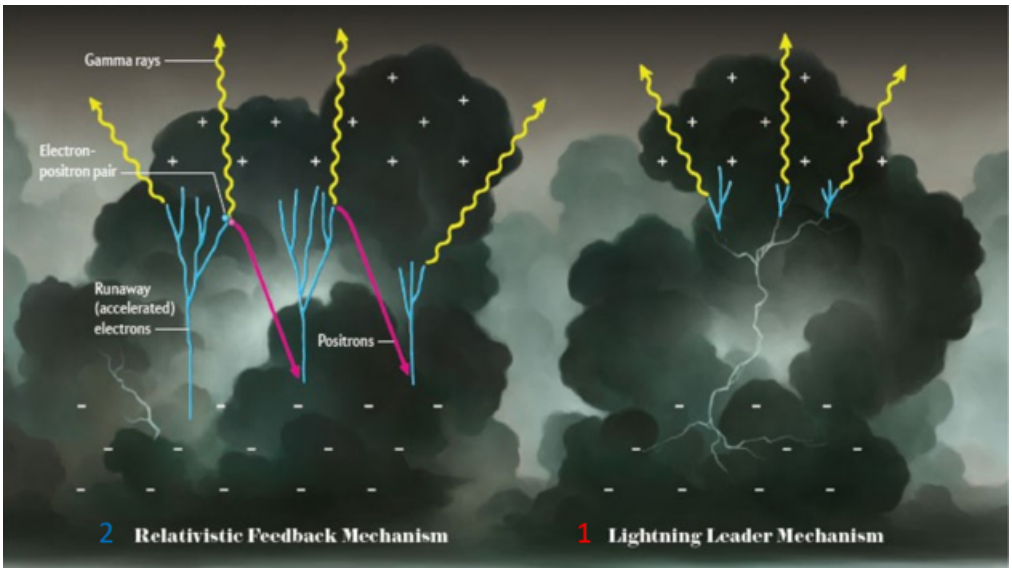

Figure 2.7. Left: Feedback mechanism using back-scattered positrons to seed new avalanches to produce the photons observed in a TGF from only the strength of the ambient electric field. Right: Lightning leader mechanism utilizing the strength of the electric field around the tips of the lightning step leaders to produce TGFs.

The second TGF production mechanism, the Lightning Leader model, has a direct relation to lightning activity within a storm. Lightning is a result of the movement of large amounts of charge between two oppositely charged regions of a thunderstorm. IC lightning is initiated between the typically positively charged upper portion of a cloud and negatively charged lower half of the cloud. CG lightning is initiated between the charged cloud (either positive or negative) and the Earth. Commonly, CG is the result of the negative charge in the lower portion of the cloud moving downward to the positively charged ground. This type of lightning strike is called downward negative CG lightning. A lightning flash begins with the lightning leader, a collection of charge from one region, taking steps toward an opposite charge region. For a typical negative CG lightning stroke, the stepped leader

process can take up to 35 ms, with steps 50 m in length and up to 50 μs apart (Rakov et al., 2003). After these steps make a complete connection, the return stoke occurs producing a radio signal as the total charge from the cloud is now connected and free flowing to the Earth. The Lightning Leader mechanism involves RREA as a result of thermal electrons being accelerated to relativistic energies by the very strong small-scale electric fields at the tip of the lightning leader channel that are the result of the large amount of charge confined to the narrow, rounded tip of the leader (Celestin et al., 2011; Xu et al., 2012). With multiple leader steps producing these avalanches, photon fluxes similar to that of TGFs can be observed. In this scenario, TGFs would require the stronger electric field from the leader tips than the ambient field and would thus be emitted prior to the strong optical emission produced by the return stroke. In the scenario of searching for bursts from the ground, the negative CG lightning is of interest in order to accelerate the electrons downward toward the detectors; however, with an opposite polarity strike positrons will be accelerated in the direction of the detectors, which can yield the ability to observe the positron annihilation 511 keV line. It is also possible that a combination of both the lightning leader and feedback mechanisms can explain the production of TGFs.

Chapter 3. TETRA-II Equipment

TETRA-II is an array of Bismuth Germanate (BGO) scintillators located at Louisiana State University in Baton Rouge, Louisiana (LSU), the University of Puerto Rico in Utuado (UPRU), and the Centro Nacional de Metrologiá de Panamá (CENAMEP) in Panama City, Panama. Locations were chosen due to their high lightning rate, available infrastructure, and, in the case of Panama and Puerto Rico, their locations below the Fermi satellite orbit. In Utuado, ten detector boxes containing 58 BGO scintillators were deployed on the roof of Building B at UPRU (18.25°, -66.72°), approximately 25 km from the Atlantic coast on the northern slopes of the Cordillera Central Mountains at an altitude of 180 m. Each box is separated by approximately 15 m lining two sides of the roof top, with a maximum distance between boxes of ∼65 m. In Baton Rouge, three detector boxes were mounted directly next to each other on the roof of the LSU Physics & Astronomy building (30.41°, -91.17°) approximately 125 km inland from the Gulf of Mexico at an altitude of 15 m above sea level. Five Panama City detector boxes were mounted on the roof of CENAMEP (9.00°, -79.58°) 60 km from the Atlantic coast and 10 km from the Pacific coast at an altitude of 30 m. These boxes are separated by 7 - 15 m.

The 18 detector boxes each contain five or six $25.4 \times 2.5 \times 2.5$ cm^3 BGO scintillators capable of detecting gamma-rays over the range 200 keV - 10 MeV. Each individual scintillator is wrapped in teflon and aluminum (Al) foil and viewed by two 3.8 cm diameter Hamamatsu R11102 photomultipliers (PMTs), one at each end, with green sensitivity matched to the BGO output spectrum. One PMT is mounted on each end of the BGO, held in place by a spring and mounted into a PVC tube for protection, as shown in Figure 3.1. Energy calibrations were performed using various gamma-ray sources, including Na^{22} (511 keV, 1.2 MeV), Cs^{137} (662 keV), and thoriated tungsten welding rods (239 keV up to 2.6 MeV), as well as with background peaks seen at each location. At each site, one BGO has been removed from a single box while keeping the remainder of the power and electronics chain active, thereby allowing one electronics channel to monitor for electronic noise. The

use of these BGO, as opposed to the NaI in TETRA-I, allows for an energy range up to ∼8 - 10 MeV, the minimum energy desired to compare with the modeled RREA spectrum.

Figure 3.1. The PVC assembly containing a BGO crystal viewed by 2 PMTs. The system is spring mounted with a PVC tube with PVC collars to support the BGO and PMTs.

Each box is divided into two separate devices, each device with its own front-end amplifier-shaper-trigger board and its own National Instruments (NI) 6351 PCIe high speed (1 Msample/s) data acquisition card handling 3 BGO (6 PMTs). This allows a readout of all PMTs every 13 μs. Each box has a single Field Programmable Gate Array (FPGA) board that handles the logic of the triggering system. A device triggers on coincident signals from a pair of PMTs viewing any single BGO above a ∼200 keV threshold or on a GPS pulse-per-second (PPS). Figure A.1 shows the individual front end channel schematic. When one of the trigger conditions is met, pulse heights for all of the device PMTs and GPS along with a counter timestamp are recorded. Timing is determined from a 20 MHz clock, with the PPS used for realignment every second.

A 27 V power supply provides the power needed to run all of the electronics inside a box, as well as power the high voltage supply needed for the PMTs. A schematic of the power layout is found in Figure A.2. The detectors are housed in weather-proof plastic boxes and connected to a pair of 12 V marine car batteries to supply power to the equipment in case of local power outages. Figure 3.2 shows a photograph of the interior of a fully assembled box.

The data collection software is written in LabView, and writes data to files every 10 minutes that are stored locally at the box. The raw data are written as .tdms filetypes,

Figure 3.2. The interior of a fully assembled TETRA-II box. The six BGO are seen at the top, with the electronics at the opposite end. Each box is roughly $160 \times 70 \times 80$ cm.

which allows for Direct Memory Access with significantly faster write times. Starting a file each 10 minutes gives a new GPS GPGGA (global positioning system fix data) string containing the satellite GPS timing information to be read in to realign the timing, and limits the dead time during the opening and writing between consecutive files. Individual files that do not obtain a GPS lock for timing accuracy are ignored. Each device produces a set of 4 files when writing data: 3 containing timestamp information for the BGO and GPS and 1 containing the analog channel information. Every hour all newly created files are passed to a server at LSU using a WinSCP (open source software for transferring files) script. Once a day, the raw binary tdms files that are produced by LabView are processed in a Python project that converts the counter timestamps recorded from the 20 MHz clock into UTC timestamps for analysis. For further information on the conversion of the raw tdms files to the usable timestamps, see Appendix B.

The data analysis searches for event candidates in each device by binning the entire day in 2 ms bins and selecting events exceeding 20 standard deviations (σ) above the

daily background average in both devices in a single box. This is done separately for each device since each has its own typical background rate. If two devices in a single box see a candidate that meets this 20 σ criterion, the remaining devices at the location are further examined. The event candidate times are compared with radio data from the VAISALA National Lightning Detection Network (NLDN), the VAISALA Global Lightning Dataset (GLD360), and WWLLN. NLDN data are used for comparison with LSU, GLD360 for Utuado and Panama, and WWLLN for all locations.

The 20 σ threshold was determined initially from the previous TETRA-I results (Ringuette et al., 2013) and confirmed for TETRA-II as the point where events associated with nearby lightning begin to stand out above the typical background. Figure 3.3 shows the number of 2 ms bins observed in each device versus the significance over the background rate for data within 5 s and 8 km of a lightning strike observed by the NLDN or GLD360 (dark line) commercial lightning alert networks and for all data (shaded grey). The grey background data are normalized to the same live time ($\sim$36 hrs) as the data with nearby lightning. As shown in the inset, the black (nearby lightning) data begin to exceed the grey (background) data near 20 σ. When account is taken for the fact that a single event must register in multiple devices (up to a maximum of 6 devices in 4 boxes spaced up to a maximum distance of approximately 20 m in the event on 22 October 2018 in Panama), 23 separate events satisfy the 20 σ threshold condition.

In parallel with the analysis searching for two devices in a single box above the 20 σ threshold, a second search method is performed looking for a single device with more than 5 counts in a single 1 ms bin. This removes the requirement that both devices must observe the event. If a single device at a location observes a candidate above this threshold, all the remaining devices at the location are checked. This second search has found the same 23 events.

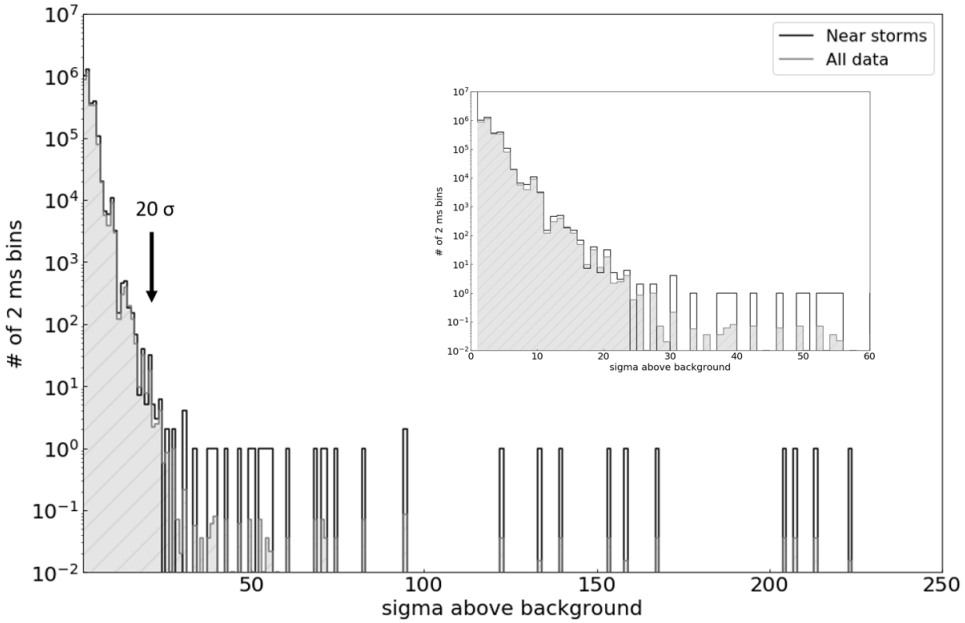

Figure 3.3. Number of 2 ms bins in a single device vs significance above daily background. Black line shows events within 5 s and 8 km of a lightning strike ("near lightning" events); shaded grey shows all data ("background") normalized to the same live time as the "near lightning" sample ($\sim$ 36 hrs). An excess of events associated with lightning is seen for $\sigma \geq 20$. Events are plotted for $\sigma \geq 1$ only.

The event candidates' ADC channels are then checked for electronic noise during the day and time of the event candidates, and channels are converted into energies using the calibration equations determined with the radioactive sources and background peaks.

In addition to the BGO, LaBr and plastic scintillators have been installed. First, at LSU a charged particle detector has been constructed using three $0.65 \times 20.3 \times 30.5$ cm^3 plastic scintillators placed inside a wooden pyramid structure with the interior painted white. At the top sit two 3.8 cm PMTs that collect the photons from the plastic. This has been placed directly on top of a set of BGO in one of the detector boxes, and is able to detect charged particles that could be triggering the system as opposed to the photons of interest.

A set of LaBr scintillators have been installed in two separate boxes on the rooftop at LSU. As of May 2019, there are 16 LaBr calibrated and taking data. These high resolution detectors will allow for observation of individual radiation lines below 1.5 MeV, with the

goals of observing radioactive radon daughters in the atmosphere being washed out to the ground by rainfall as seen in TETRA-I (Ringuette et al., 2013) and searching for the 511 keV line from electron-positron annihilation during thunderstorms. Further discussion of the LaBr is presented in Chapter 5.

In addition to the scintillation detectors, additional equipment has been installed to create a unique set of data to study the observed events. At both LSU and Puerto Rico a Boltek electric field mill (EFM) and a Vantage Pro2 Precision Weather Station have been installed. The electric field mills will allow for measurement of changes in the electric field as storms pass by each location. The weather station will act in a similar fashion, giving added information about temperature, humidity, wind speed and direction, along with other weather related data at our specific locations of interest. A final piece of equipment that was installed at LSU in May 2019 is an optical camera and microphone system. When completed, a set of 3 - 4 optical cameras will be used to cover the entire sky and monitor for lightning strikes. An initial test was concluded in April 2019 and a first image of a lightning strike has been recorded. Using a time-stamped image of a lightning strike, along with the audio of the thunder recorded by the microphone will allow for a better observation and distance estimate of individual lightning strikes using the speed of light and sound in air. Being able to better correlate the TETRA-II gamma-ray events to individual lightning strikes will assist in a better understanding of the possible production mechanisms of these events. Each of these pieces of equipment will add to the full story of information to be used to describe the thunderstorms and conditions that are seen during times when events are observed.

Chapter 4. Short Duration Observations

TETRA-II began operation in Fall 2015 with the installation of two boxes at LSU, with the remaining locations becoming operational over the next 18 months. To date, TETRA-II has detected 23 bursts of gamma-rays in Louisiana, Panama, and Puerto Rico (Table 4.1) typically ranging in duration from 0.1 - 2 ms. (Initially, two detector boxes were installed in Huntsville, Alabama. After no events were seen in Huntsville in 2 years, the detectors were removed from Huntsville in Fall 2018.) Once an event is found, the time stamp is compared with the lightning catalogs, searching for a coincident NLDN, GLD360, or WWLLN strike within 8 km of the detector location and 5 s of the trigger time. Of the 23 events detected, 19 have a radio sferic detection within 6 km and 1.5 ms of the beginning of the gamma-ray event (Table 4.2). In every case, the radio signal is reported after the start of the gamma-ray event, usually close to or at the end of the event.

Table 4.1. Number of events and operating time for each location.

Location	Live Time	# of Events
Baton Rouge, Louisiana	3 years	13
Utuado, Puerto Rico	2.5 years	1
Huntsville, Alabama	2 years	0
City of Knowledge, Panama	1.5 years	9

Of the 13 events TETRA-II detected at LSU, 11 were accompanied by an NLDN strike within 1.0 km and 1.0 ms (Table 4.2). Ten of the reported strikes were negative polarity cloud-to-ground (CG) strikes, with peak currents ranging from -22.3 kA to -111.4 kA, while the event on 15 March 2019 had an IC strike reported by NLDN at the end of the burst. Two LSU events had no associated radio signal: 170707 occurred during a time of reported rainfall, but no lightning activity, and 180915 is the weakest event seen in Table 4.2.

Figure 4.1 shows one of three events from the detectors at LSU on 25 Mar 2017. Time zero is defined as the first 50 μs bin with ≥ 2 counts. The radio signal is labelled by the plus sign, with the distance to the radio event given on the right-hand axis. The burst was

Table 4.2. TETRA-II event properties. Counts (number of photons) in events are included. Duration is defined as time from the first to the last photon. Δt is defined as the time difference between the radio sferic and t_0. Lightning distance is given as the distance to the radio position, and I_P is the peak current determined from the radio measurement.

Event	Location	Timestamp UTC	Counts	Duration (μs)	Δt (μs)	Lightning Distance (km)	Lightning Source	I_P (kA)
160427	LSU	16:49:25.418	19	100	20	1.0	NLDN	-111.4
160919	Utuado	18:09:33.762	183	800	530	2.6	GLD360	-16.6
170307	LSU	23:34:30.446	169	700	50	0.5	NLDN	-66.4
170325a	LSU	15:47:15.270	73	500	470	0.2	NLDN	-22.3
170325b	LSU	16:02:12.737	29	450	460	0.4	NLDN	-51.7
170325c	LSU	16:02:12.918	61	250	230	0.4	NLDN	-32.6
170601	Panama	01:15:24.179	23	850	700	5.9	GLD360	-51.1
170624a	LSU	19:34:50.268	203	1150	1080	0.4	NLDN	-43.5
170624b	LSU	19:34:50.475	133	400	350	0.5	NLDN	-32.7
170624c	LSU	19:34:50.364	48	100	10	0.5	NLDN	-36.6
170707	LSU	22:25:51.186	113	5950	*	*	*	*
170810a	Panama	14:34:01.703	91	1350	1300	0.6	GLD360	-139.5
170810b	Panama	14:34:01.684	19	350	*	*	*	*
171018a	Panama	17:43:46.565	97	1550	1180	2.5	GLD360	55.9
171018b	Panama	17:45:31.545	34	900	850	2.9	GLD360	-67.1
171103	Panama	19:34:30.382	25	350	190	6.5	WWLLN	*
171204	Panama	17:54:50.349	24	1750	880	3.5	GLD360	-22.5
180605	Panama	11:59:21.008	44	650	590	6.8	WWLLN	*
180815	LSU	22:56:43.222	56	950	900	0.2	NLDN	-25.6
180817	LSU	13:51:59.767	45	650	500	0.5	NLDN	-95.0
180915	LSU	20:42:56.859	15	500	*	*	*	*
181022	Panama	21:54:00.386	89	1000	1030	6.1	GLD360	-113.8
190315	LSU	08:11:21.506	99	500	360	1.4	NLDN	16.2

* No reported values

seen to build up over its ∼500 μs duration, and then promptly cut off after its peak, 50 μs before the NLDN radio signal.

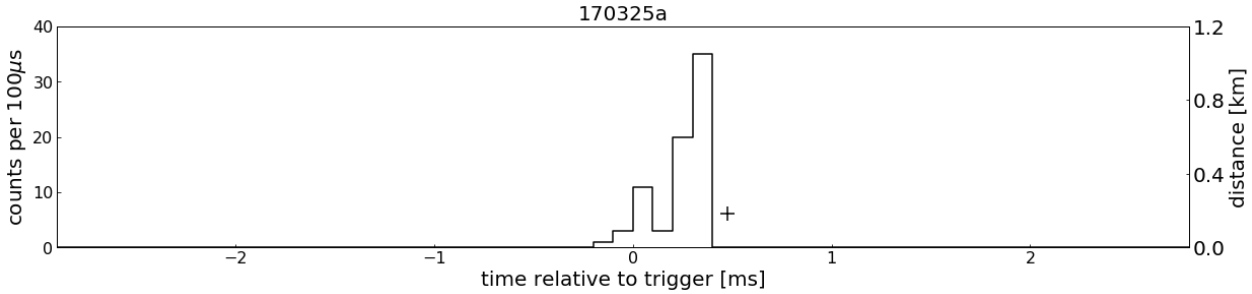

Figure 4.1. Time series of photons observed over a 6 ms window binned in 100 μs bins for the LSU event at 15:47:15 UTC on 25 March 2017, summed over the 11 BGO in the two boxes. The lightning radio signal is represented by the +.

GLD360 data were used to study the correlation between RF sferic and TETRA-II gamma-ray events for both Utuado and Panama City. Of the nine events seen in Panama, five have a GLD360 strike within 2 ms from the beginning of the event and within 6.5 km of the detectors, four associated with negative polarity lightning and one with a positive polarity stroke. Three of the Panama events were associated with a WWLLN strike within 0.6 ms of the beginning of the gamma-ray trigger and within 7 km. The one Panama event, 170810b, that was not associated with a lightning strike did occur during a thunderstorm and was detected within 100 ms of another event, 170810a.

Figure 4.2 shows the event at CENAMEP in Panama on 1 June 2017. This event is roughly symmetrical in shape over the ∼500 μs duration of the main peak. In this case, the radio signal observed from GLD360 is reported ∼100 μs after the peak of the burst.

The single event seen at the University of Puerto Rico in Utuado on 19 September 2016 is seen in Figure 4.3. This event was seen in 4 boxes across the rooftop, ranging up to approximately 50 m apart. Here, the event is seen building up before the negative polarity radio signal is observed over 500 μs after the start of the event. The event ends soon after.

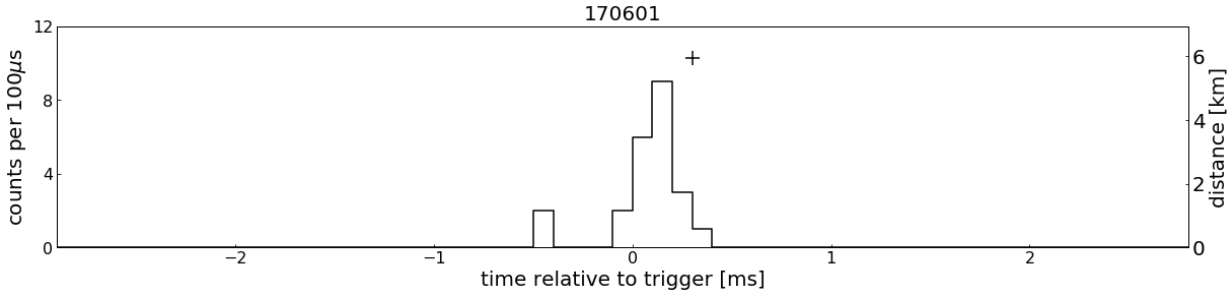

Figure 4.2. Time series over a 6 ms window binned in 100 μs bins for the Panama event at 01:15:24 UTC on 1 June 2017, summed over all BGO in three boxes. The lightning radio signal is represented by the +.

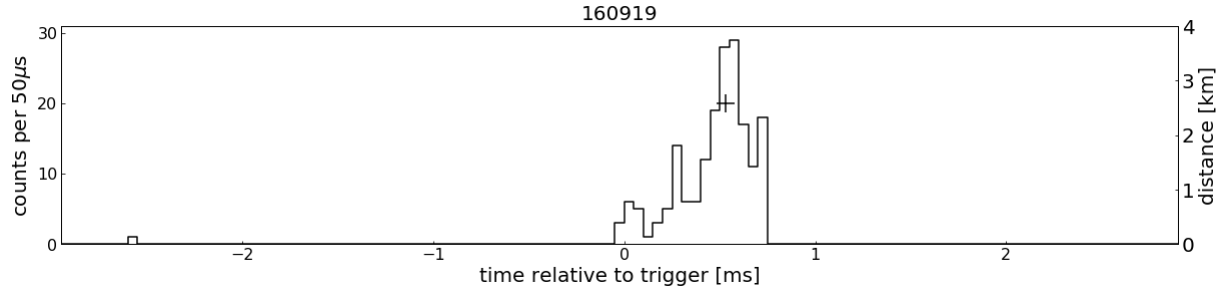

Figure 4.3. Time series over a 6 ms window binned in 50 μs bins for the Puerto Rico event at 18:09:33 UTC on 19 September 2016, summed over all BGO in four boxes. The lightning radio signal is represented by the +.

An average energy spectrum summed over 23 events is presented in Figure 4.4. Energies were determined by converting the recorded ADC values using the calibration data from known x-ray sources and cosmic ray muons. The ADC was observed to behave linearly up to 10 MeV. Energy deposits up to 6 MeV are seen. Figure 4.5 shows the time series for all 23 events over 6 μs windows in 50 μs time bins.

Eleven events show a similar structure to that in Figure 4.1 with the burst building up and then terminating shortly after its peak, with the radio signal following. This structure suggests bursts emitted by individual lightning leader steps as they move downward toward the detectors. As each step approaches, the number of photons detected increases until the gamma-ray production is terminated by the stroke hitting the ground, followed by the return stroke accompanied by the RF emission.

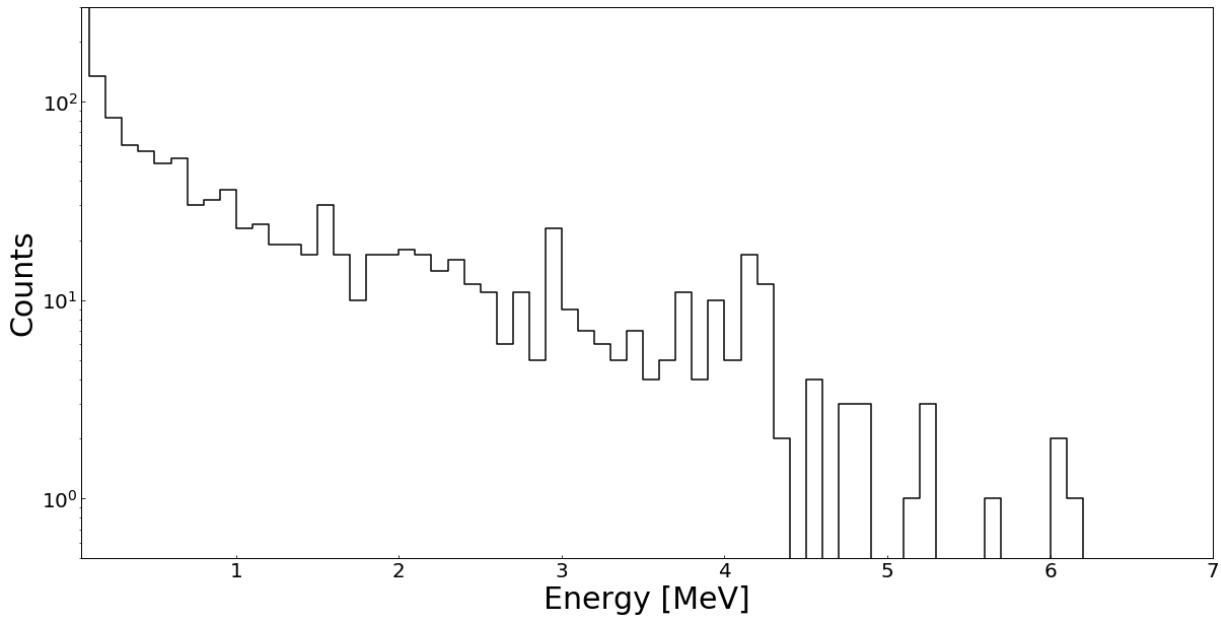

Figure 4.4. Summed energy spectrum of 23 TETRA-II events.

For all the observed TETRA-II events with an associated lightning strike, Table 4.2 shows a positive time offset Δt between t_0 of the gamma-ray signal and the radio sferic time with $\Delta t \leq 3$ ms in every case. Based on the typical duration of the leader process, this suggests that these events are not only produced by the lightning leader, but during the last stages of the channel development before the first return stroke.

One unique event is shown in Figure 4.6. This event, detected on 7 July 2017 at LSU, shows a sharp spike at the beginning of the event and then a long tail lasting up to 6 ms. No sferic was reported in association with this event. Assuming the bursts observed by TETRA-II are beamed with half-angle $\delta\Theta$, as is seen from space, where $\delta\Theta \sim 30°$(Connaughton et al., 2010), then this event can be understood as an event directed away from the detectors but at an angle $< \delta\Theta$ with respect to TETRA-II; in this case, successive leaders are farther from the detector and the number of gamma-rays detected decreases with increasing time and distance. The red curve shown in Figure 4.6 is a $1 / t^2$ that aligns well with the data observed. This would be expected given a constant intensity emission during each leader step. This agreement was seen in the upward stepping events

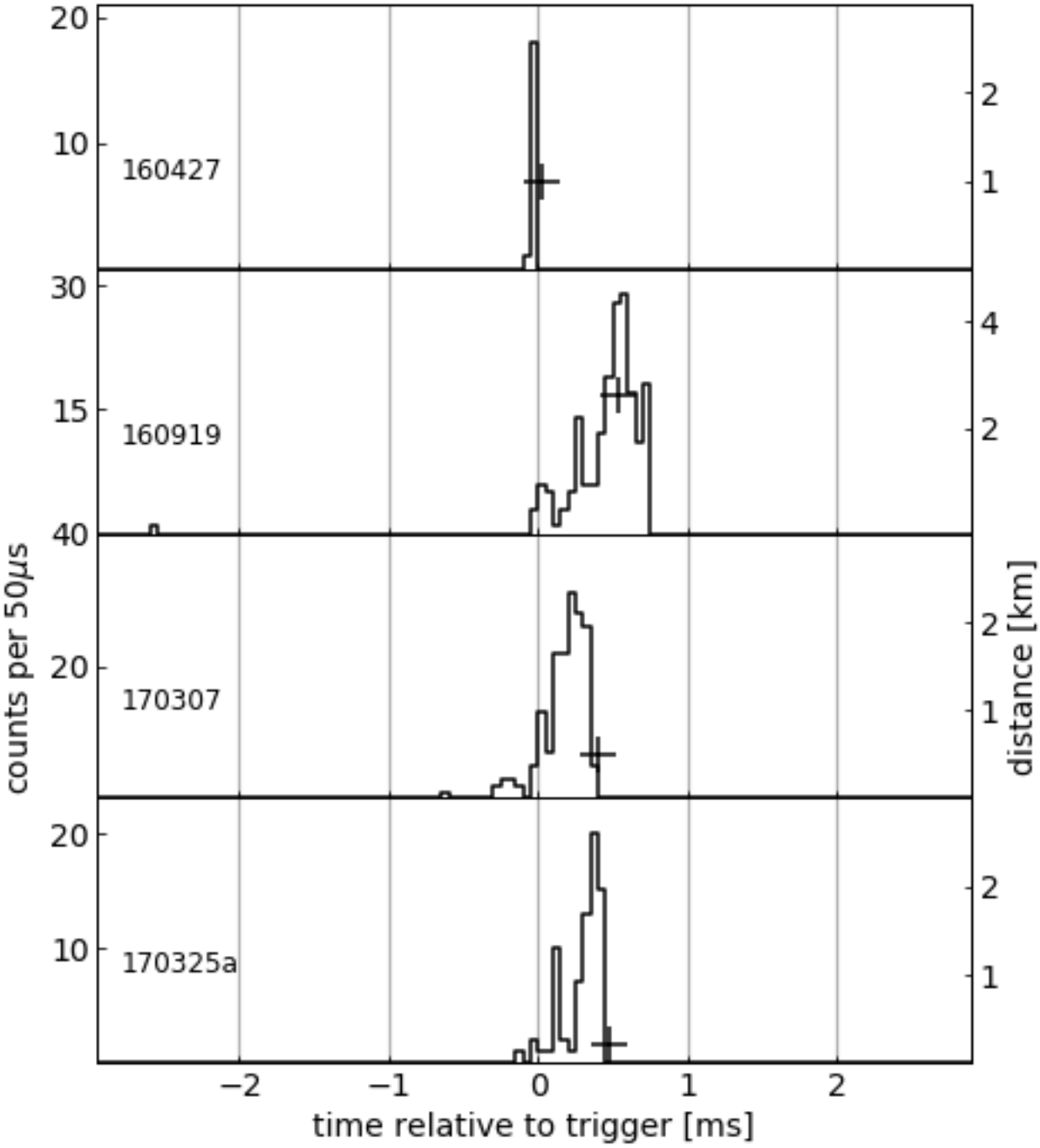

Figure 4.5. Time series of 4 bursts over a 6 ms window binned in 50 μs bins. The lightning radio signals are represented by the +.

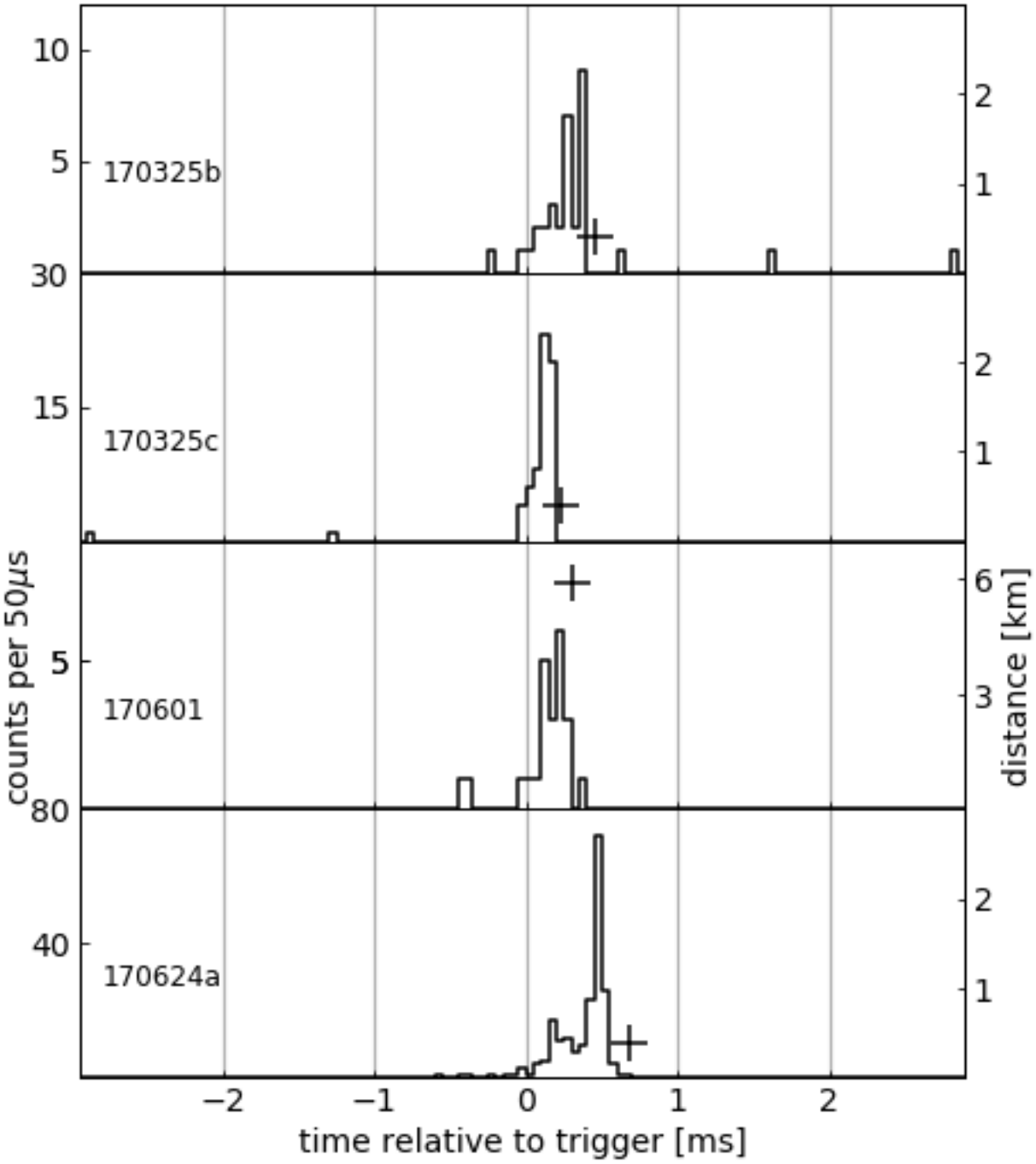

Figure 4.5. Time series of 4 bursts over a 6 ms window binned in 50 μs bins. The lightning radio signals are represented by the +.

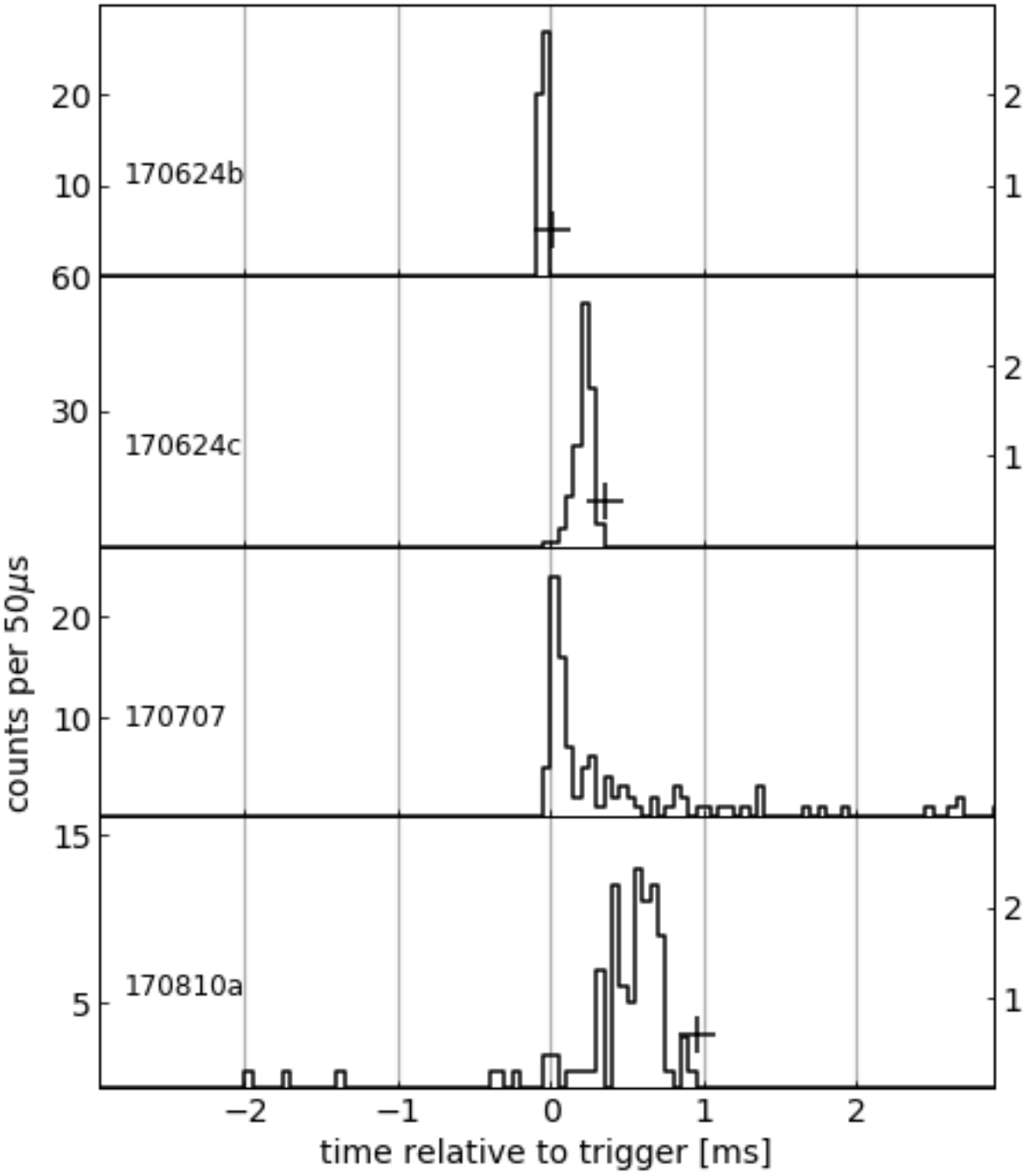

Figure 4.5. Time series of 4 bursts over a 6 ms window binned in 50 μs bins. The lightning radio signals are represented by the +.

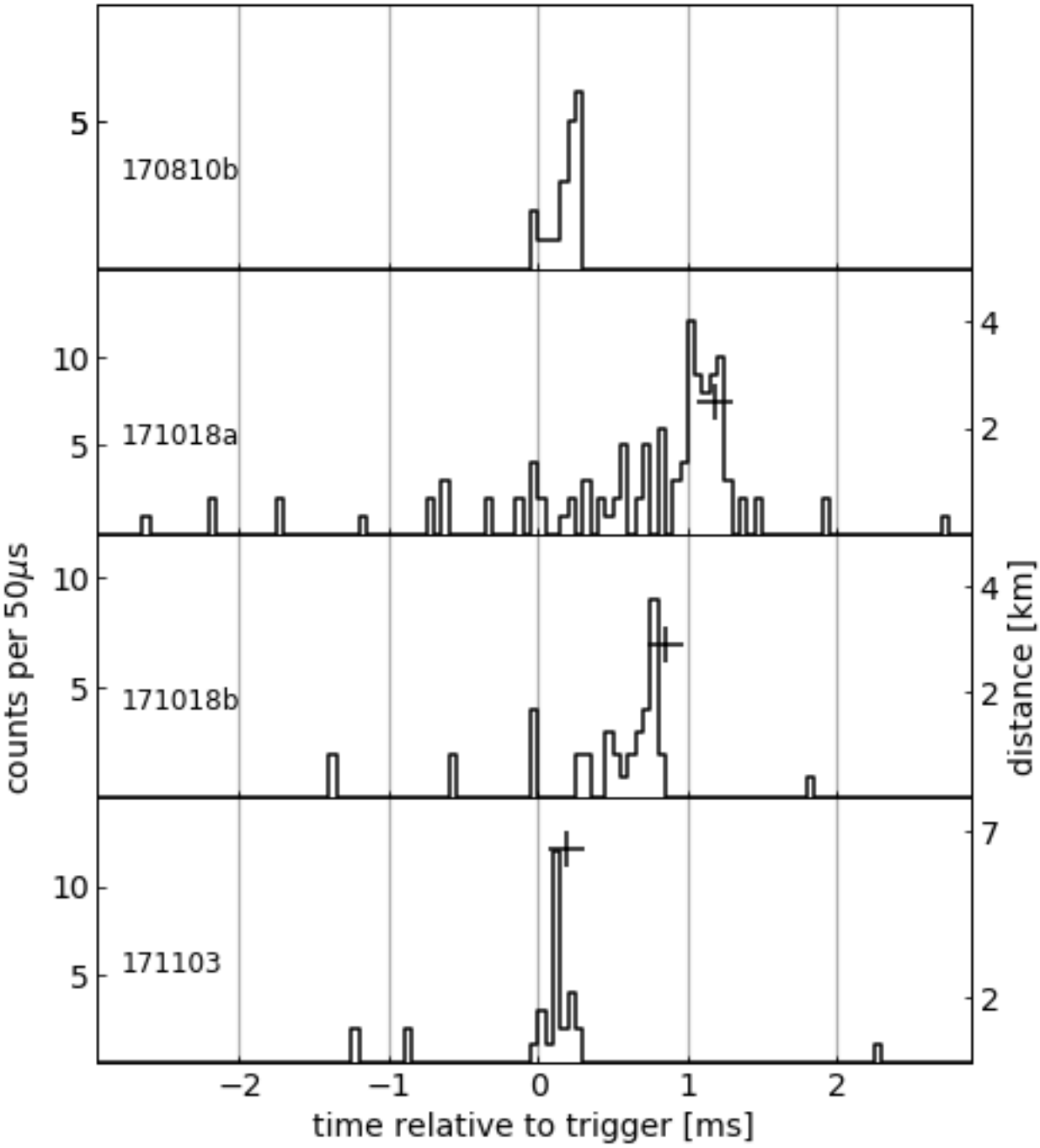

Figure 4.5. Time series of 4 bursts over a 6 ms window binned in 50 μs bins. The lightning radio signals are represented by the +.

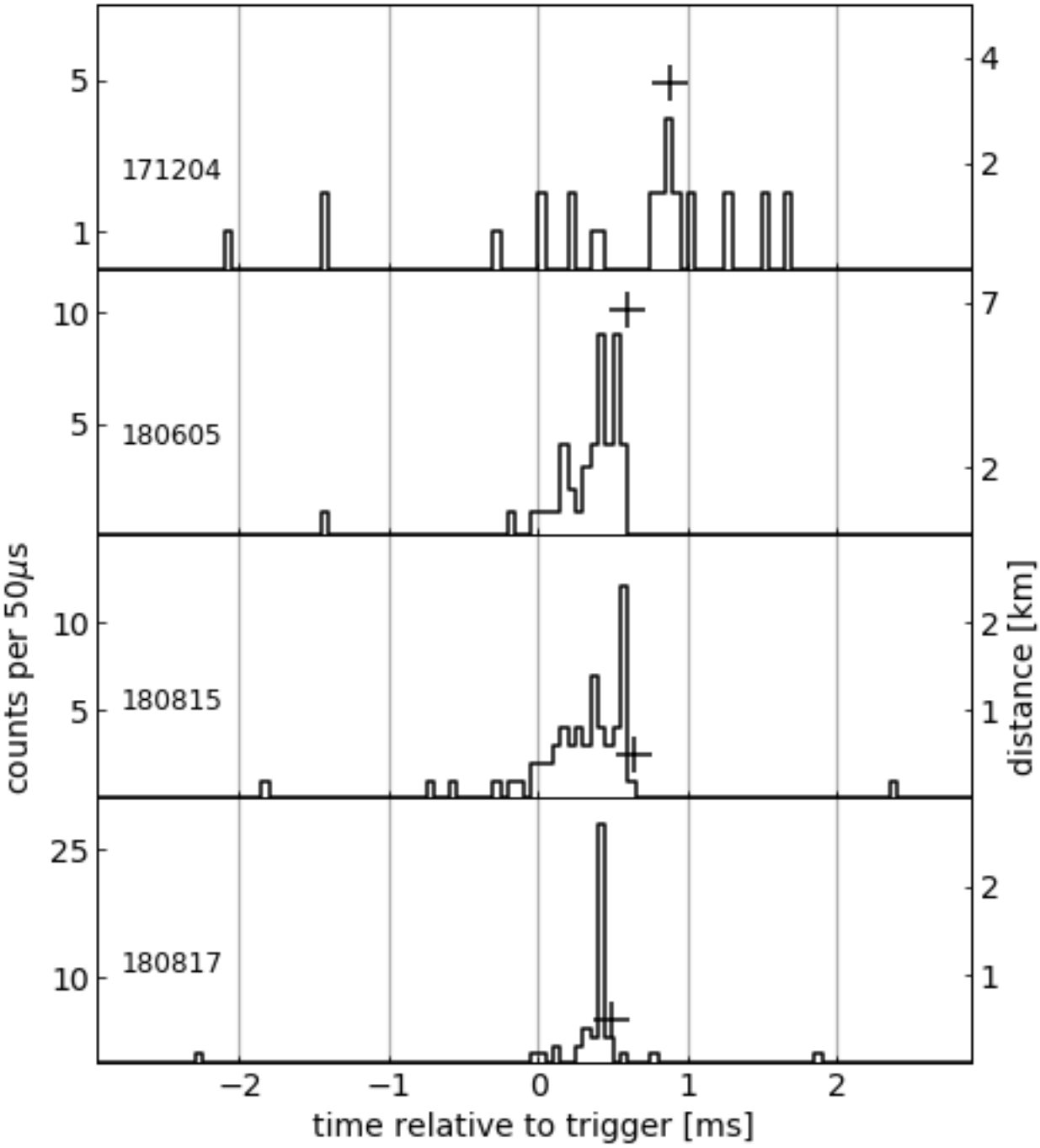

Figure 4.5. Time series of 4 bursts over a 6 ms window binned in 50 μs bins. The lightning radio signals are represented by the +.

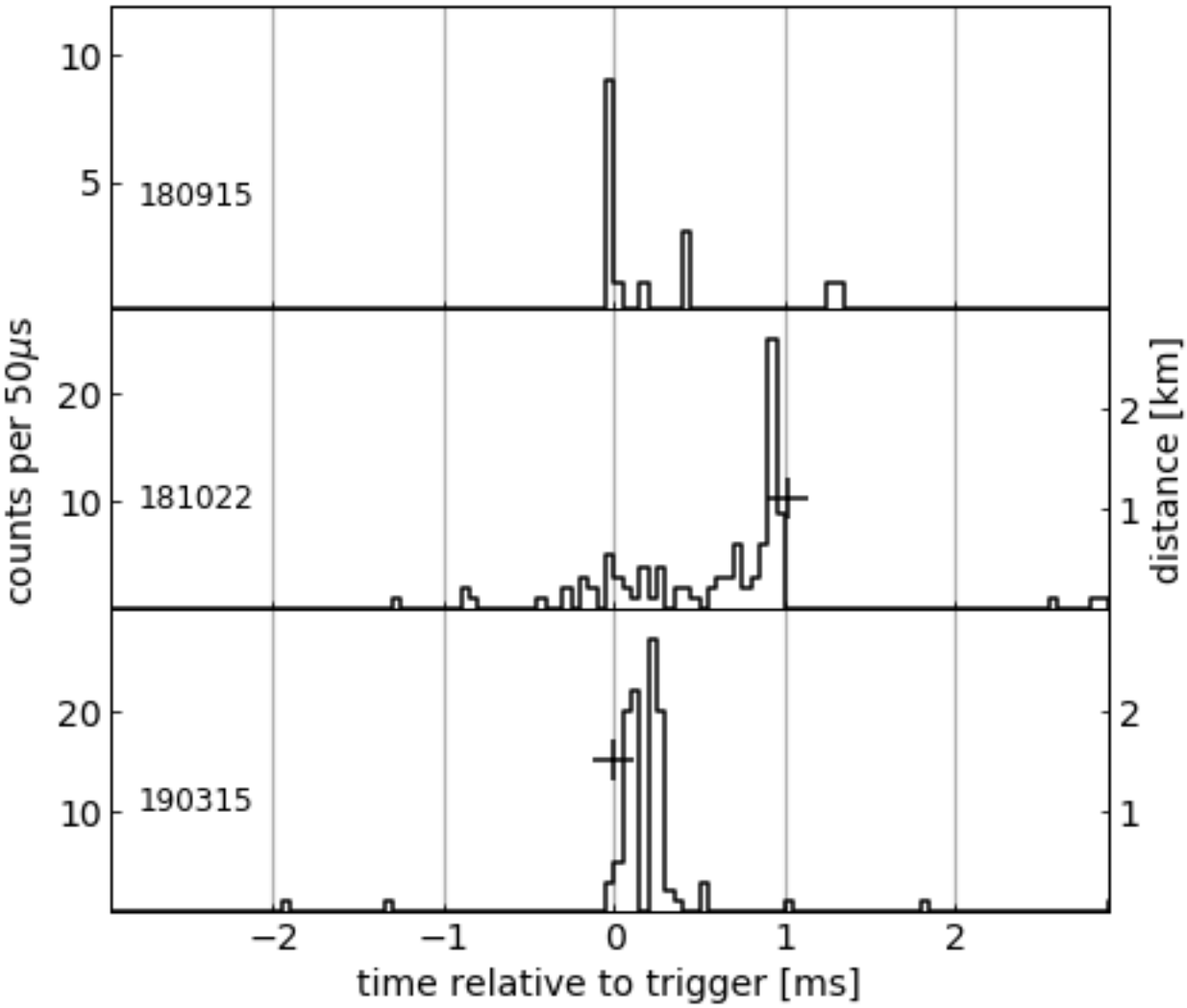

Figure 4.5. Time series of 3 bursts over a 6 ms window binned in 50 μs bins. The lightning radio signals are represented by the +.

as well. Figure 4.7 shows two of these such events, 170624a and 170624c, with the 1 / t^2 curve.

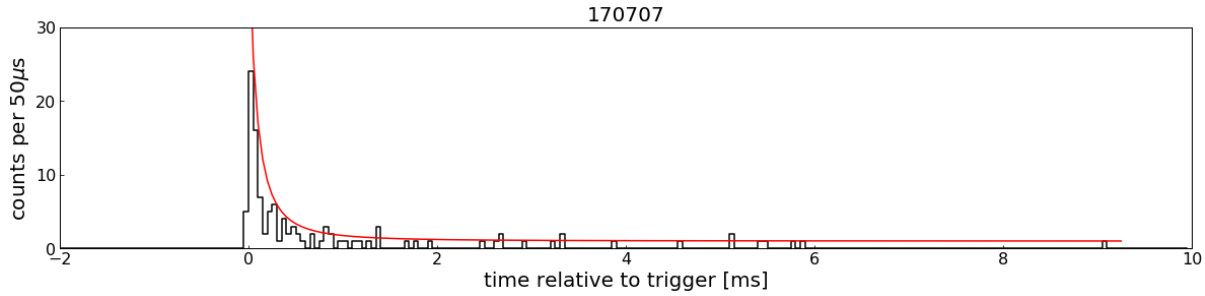

Figure 4.6. Time series over a 20 ms window binned in 100 μs bins for the LSU event at 22:24:51 UTC on 7 July 2017. 1 / t^2 curve shown in red.

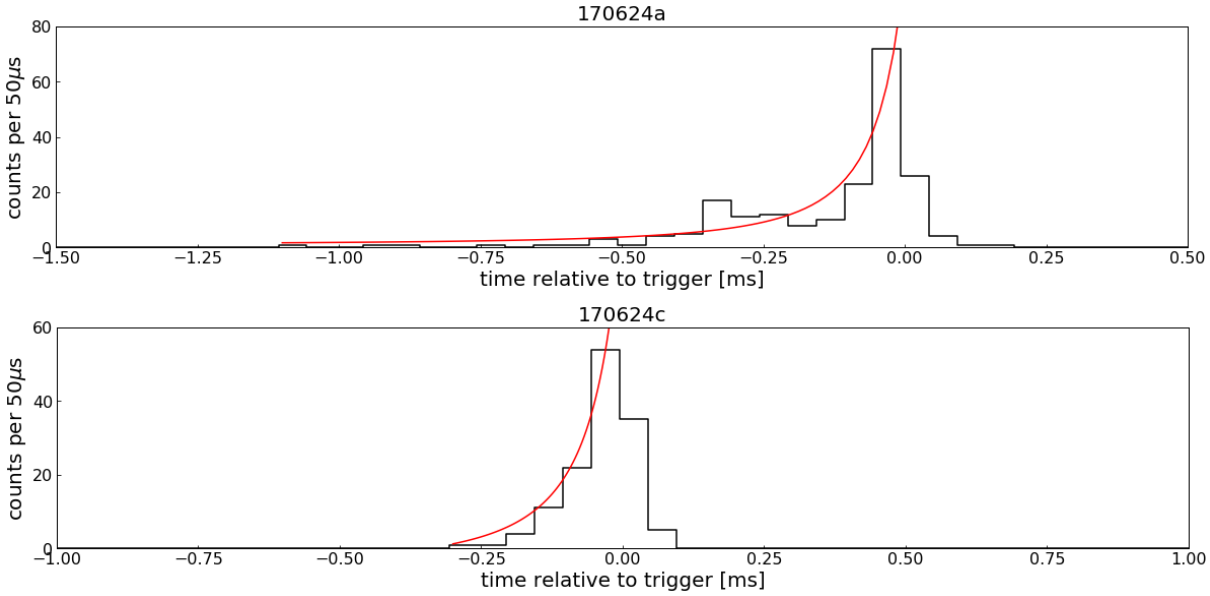

Figure 4.7. Time series over a 5 ms window binned in 50 μs bins for 2 LSU events on 7 July 2017. The red curve in each is a 1 / t^2 curve that is expected with a uniform intensity of emission at each step in the leader process.

X-ray emission associated with lightning leaders has been reported by others (Dwyer, 2005; Mallick et al., 2012), but with distinct differences compared to the events presented here. Table 4.2 shows the duration of a TETRA-II event ranges up to over 1 ms, longer than that of the X-ray observations that contain short ten-to-hundred microsecond duration pulses. Dwyer et al. (2012) observed, along with a TGF after a lightning return stroke,

a collection of x-ray hits that were abruptly cut off at the moment of the lightning return stroke. These x-ray emissions due to the local high electric fields from the lightning leaders, on scales of tens to hundreds of microseconds (Dwyer et al., 2004b), were seen by their collection of 23 NaI scintillators, each 7.6 cm × 7.6 cm and appear similar to what is observed by TETRA-II.

Mallick et al. (2012) reported multiple lightning flashes with similar x-ray emission associated with lightning strikes, typically with energies below 1 MeV. The largest x-ray burst observed by Mallick et al. (2012) lasted ∼200 μs with measured energies up to ∼5 MeV, similar to the TETRA-II event in Figure 4.8. One distinct difference: The peak of 170624a was observed less than 100 μs before the initial lightning return stroke indicating this burst was associated with the lightning leader steps near the first return stroke. The large burst reported by Mallick occurred in association with the third stroke of the lightning flash, ∼50 ms after the initial return stroke.

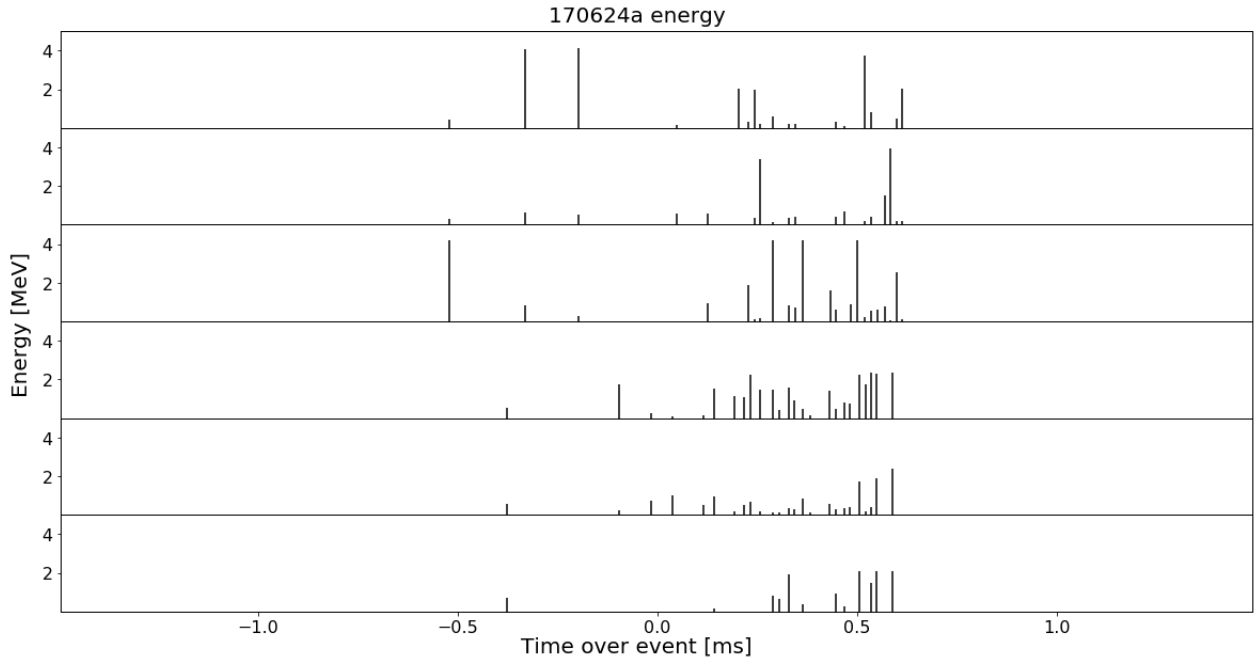

Figure 4.8. Individual BGO energy readings from event at LSU at 19:34:50 UTC on 24 June 2017. Peak energy seen up to 4 MeV over ∼1 ms.

Figure 4.9 shows the individual photon energies for an event at LSU on 15 Aug. 2017. Energies are only included in Figure 4.9 if the time between successive detector hits in a single BGO (with each photon arrival time tagged with an accuracy of 50 ns) is in excess of 13 μs, the sampling cycle time of the NI analog-to-digital converter. To monitor for X-ray pileup, a 5 mm tin (Sn) filter was placed above the BGO detectors in one of the two side-by-side Louisiana boxes in 2017. This shielding layer attenuates over 70% of X-rays at 500 keV. Figure 4.9 shows an event seen at LSU in both the box with Sn shielding (left side) and the box without (right side). Both boxes show roughly 20 counts during the duration of the event, with individual photon energies measured up to 3 MeV, and no indication of attenuation due to absorption of lower energy X-rays.

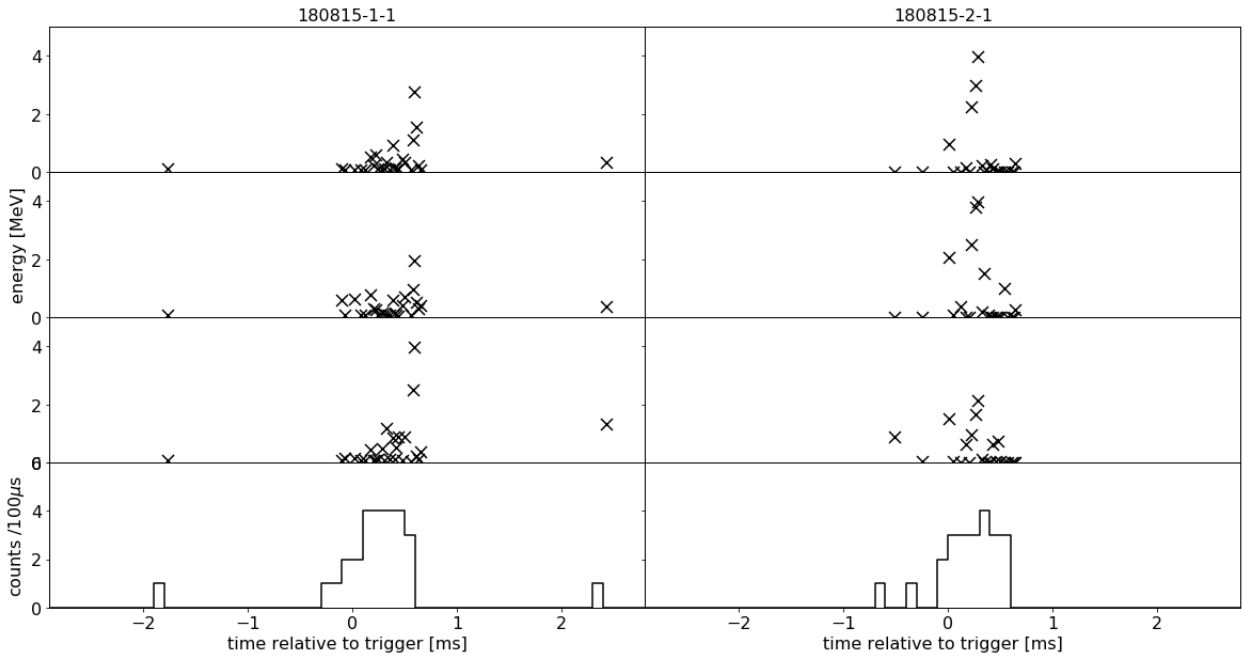

Figure 4.9. Event at LSU at 22:56:43 UTC on 15 August 2018. Left-hand plot shows box with BGO shielded by 5 mm of Sn; right-hand plot shows event seen in box without shielding.

In summary, 20 of the 23 TGF-like TETRA-II events had a lightning strike reported from at least one of NLDN, GLD360, and WWLLN. In every case, the lightning strike occurred between 13 μs and 1.3 ms after the beginning of the event, typically at the end of the gamma-ray event, indicative of the bursts being produced by the final stages of the

lightning leader stepping process. All of the lightning strikes were within 7 km, with 9 reported less than 500 m away. Out of the 18 events where the lightning polarity is known, 16 are negative and 2 were positive, and in 10 of the 11 cases where the type is known, the type is CG. Approximately half the events show the characteristic behavior illustrated in Figure 4.1, with the signal increasing over the duration of the event and then abruptly ending.

Chapter 5. Long Duration Observations

In addition to the the short sub-second events described in the previous chapter and observed by other experiments both from space and on ground, other types of longer duration events have been reported from ground based detectors. Tens of minutes to hours long duration increases in rates have been observed both at Mt. Aragats in Armenia (Chilingarian et al., 2010, 2019) and at LSU by the TETRA-I experiment (Ringuette et al., 2013). At LSU when looking at a day's worth of TETRA-I data binned in minute time bins, increases in count rate that were up to double the background rate were observed. Upon comparing these time frames with available weather radar reflectivity data, it was observed to occur during times of rainfall (Ringuette et al., 2013). The addition of high-resolution Lanthanum Bromide (LaBr) scintillators (with energy resolution less than 5% at 662 keV) made it possible to search for discrete lines during these storms. An observed TETRA-I spectrum is shown in Figure 5.1 showing the individual lines of radon daughters washed out during the rainfall.

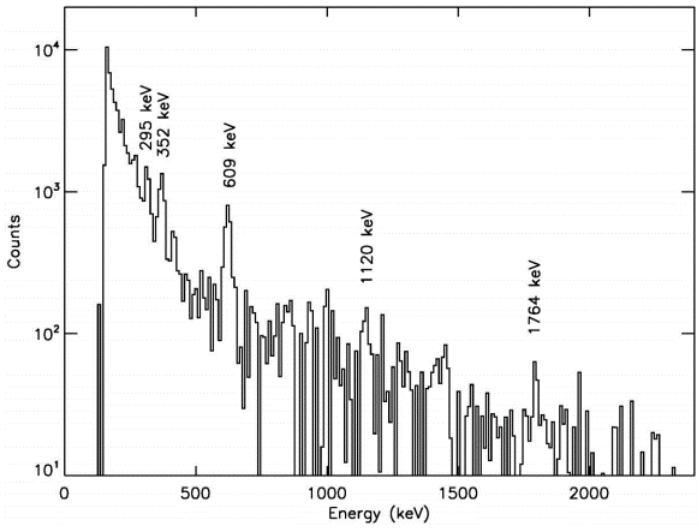

Figure 5.1. High resolution spectrum observed by TETRA-I showing the emission lines of radon daughters produced during a 4 hr rainfall event (Ringuette et al., 2013).

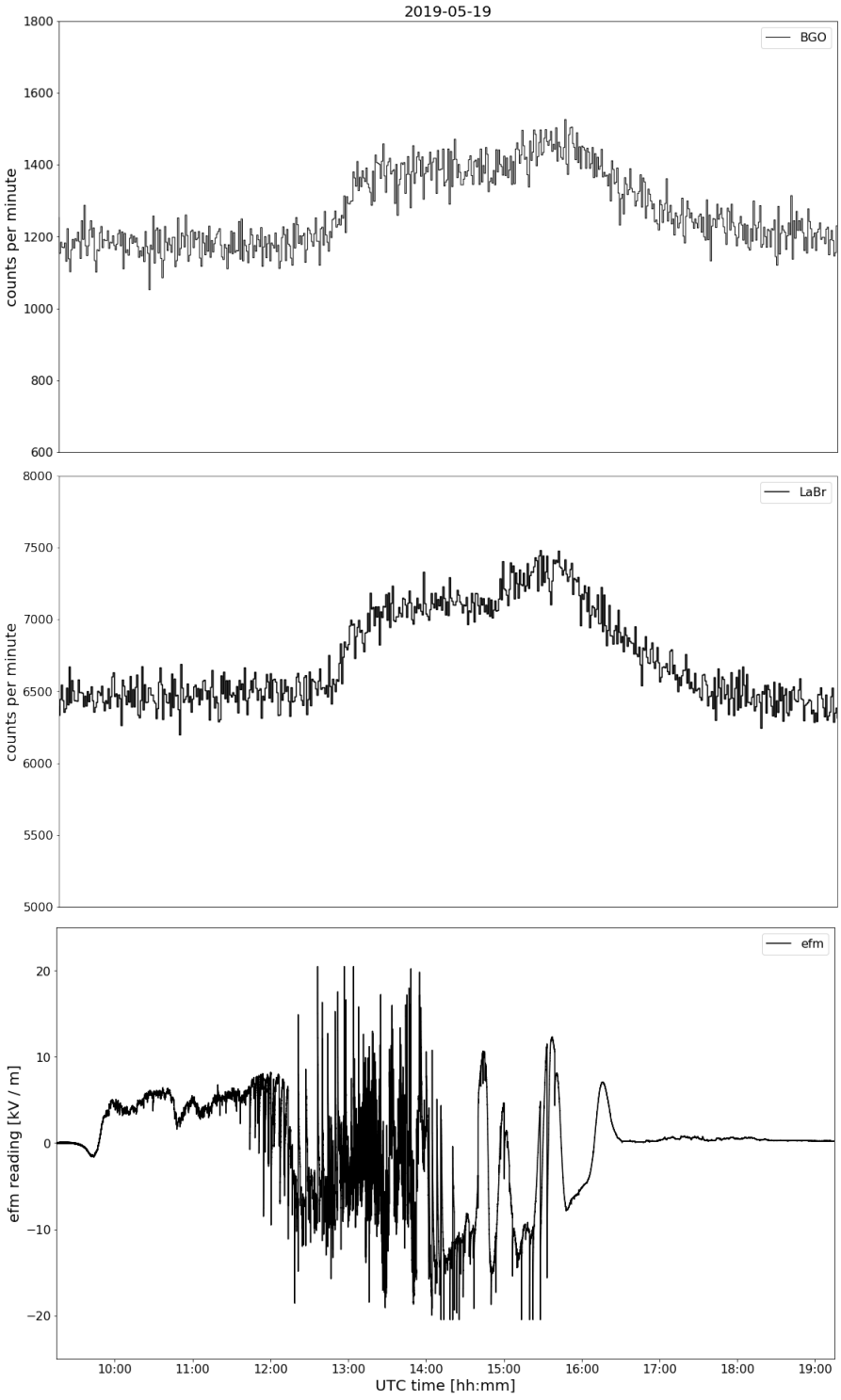

Figure 5.2. Time series at LSU on 19 May 2019 for a set of 3 BGO, a set of 4 LaBr, and the electric field mill with an enhancement in the rate seen in association with rainfall.

In March 2019 four LaBr scintillators were added to the equipment at LSU with another 12 to be added in the summer. These scintillators were installed using the TETRA-I electronics, with the focus on the better energy resolution rather than the high speed readouts of TETRA-II, to search for the radon daughter lines. Long duration increases in count rates have been observed in the BGO data at all TETRA-II locations as well as in the LaBr data at LSU. Figure 5.2 shows BGO, LaBr, and electric field data at LSU on 19 May 2019. The BGO and LaBr data are binned in minute time bins and all 3 plots are shown over the same 10 hour time window. Around mid-day UTC, an increase in the count rate was observed in both sets of detectors lasting 5 hours. This was compared with the electric field data taken from the same rooftop using a Boltek Electric Field Mill where it is seen to be an active time period indicative of lightning and cloud structures passing overhead. There was no short duration burst observed during this timeframe.

Along with these much longer enhancements, a burst in the range of hundreds of ms to minutes have been seen by a set of detectors in Japan (Enoto et al., 2017). The unique feature observed by Enoto et al. (2017) was the presence of a 511 keV emission line that lasted for a minute. Due to the electric field polarity and absence of a higher energy seed gamma-ray, along with the observation of a 10 MeV cutoff in the spectrum attributed to fast neutrons, it was concluded that this was a result of photonuclear reactions occurring in the atmosphere. The gamma-rays emitted from the lightning strike interacted with nuclei in the atmosphere, producing unstable radioactive isotopes and neutrons. These isotopes then beta decayed generating positrons which annihilated to produce the 511 keV photons that were detected.

To search for similar, longer duration, events, the TETRA-II daily data were binned in 1 second and 1 minute time bins. Transient rates that rise up above the normal fluctuations for a given day in an individual device are then compared with the remaining devices at a given location looking for coincidences. To date, 1 longer duration event candidate has been observed at LSU on 20 February 2017, seen in Figure 5.3. This burst was observed

in both devices in the only box running at the time. A sharp peak is seen followed by a tail lasting up to 200 ms. No radio signal was observed from a lightning strike during this time.

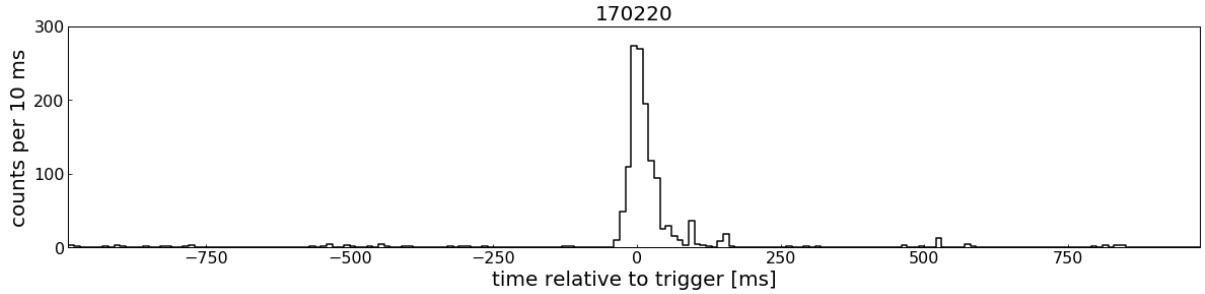

Figure 5.3. Time series over a 2 s window binned in 10 ms bins for the LSU event at 20:43:10 UTC on 20 February 2017.

Chapter 6. Conclusion

TETRA-II is an improved ground-based array of detectors to study the production mechanism of, and to search for patterns in, bursts of gamma-rays associated with thunderstorms. While catalogs have been produced from satellite instruments studying TGFs, no such catalog of thunderstorm related events has been published for ground-based events. A ground-based array makes possible detailed correlations with individual lightning strikes and storm cells due to being significantly closer to the source of the bursts. If the bursts can be correlated with specific thunderstorm characteristics (e.g., storm types, 3d radar images, cloud top heights, vertical integrated liquid density, presence of hail), it may be possible to obtain a better understanding of the storm conditions and the production mechanism. The TETRA-II experiment deployed to study these bursts is described, as well as the first TETRA-II catalog of lightning leader produced gamma-ray events.

In the original version of the experiment, TETRA-I observed 39 bursts of gamma-rays associated with lightning at LSU with an array of NaI detectors (Ringuette et al., 2013). The results presented here are a complete catalog of the twenty three events observed in the first two years of TETRA-II operation that show a similar pattern of association with nearby negative polarity lightning, with the expected increase in photons detected due to the higher density BGO scintillators. The average number of photons detected over the energy range 200 keV - 8 MeV is 70, with average burst duration 970 μs. Events were detected in multiple boxes ranging up to 50 m apart, while Ringuette et al.(2013) reported observing coincident events up to 1500 m apart indicating either a much larger beaming angle for events than would be observed with TETRA-II or a higher altitude of the source. In 20 of the bursts, the gamma-ray event started between 13 μs and 1.3 ms and ended up to 100 μs before the radio sferic, supporting the argument that these events were produced during the later stages of the lightning step leader process.

In over half of the events, a stepping structure was seen to build up before abruptly ending at the time of an associated lighting flash, suggesting that these gamma-rays were

typically produced by individual downward-moving leaders approaching the detectors. This stepping up structure, as well as the stepping down structure of 170707, agree qualitatively with a 1 / t^2 curve, which is expected with emission from individual leader steps as they approach, or move further from, the detector at constant velocity.

With over 2 years of operation at all 3 locations, only 1 of the 23 events observed was seen in Puerto Rico, where 10 detector boxes are located compared to 8 at LSU and Panama combined. A possible explanation is this is a result of geographical differences. The equipment at both LSU and Panama are nearer sea level, below 30 m altitude, while the Puerto Rico location is on the slopes of the Cordillera Central Mountains, at an altitude of ∼180 m. This could result in different storm characteristics and types or different lightning behavior affected by the mountains.

A distinct difference between the events presented here and other ground based events involves their correlation with the lightning leader process. Two observations of ground level detected events, one at the ICLRT at the University of Florida (Dwyer et al., 2012) and one at the Lightning Observatory in Gainesville, Florida (Tran et al., 2015), both involved a burst of gamma-rays lasting less than 50 μs occurring ∼200 μs after the lightning return stroke was observed. This is counter to what is observed by TETRA-II, and implies that bursts of gamma-rays produced within thunderstorms can be produced through either of the two mechanisms discussed: the lightning leader model detailed by Celestin et al.(2011) with an expected time offset between burst and radio sferic or the relativistic feedback model of Dwyer (2012) where events require only the ambient electric field, and would be independent of lightning activity.

The addition of tin shielding over half of the BGO at LSU has confirmed that what is being observed is not the pileup of lower energy x-rays. Rather, photon energies up to ∼6 MeV have been observed, lower than the characteristic ∼7 MeV energy expected from RREA. Better statistics from more events will allow for a better spectral analysis potentially up to 10 MeV.

The observation of the x-ray/gamma-ray burst preceding the lightning has been seen by other experiments as well. GBM TGFs have recently been studied in coordination with the Geostationary Lightning Mapper (GLM) (Alnussirat et al., 2019), an optical lightning detector launched in November 2016 on the The Geostationary Operational Environmental Satellite R-series 16 (GOES-R 16) satellite (Goodman et al., 2013), and the first results of ASIM have been presented at the American Geophysical Union Fall 2018 meeting (Østgaard et al., 2018). Both ASIM and GBM - GLM TGF - lightning association studies have found that TGFs are observed during the final stages of the lightning leader process.

Current plans call for TETRA-II operation for at least three more years with the recent addition of electric field mills, weather stations, optical camera and microphone systems, and high resolution LaBr scintillators to look for lines resulting from radon daughters being washed out due to rainfall and for evidence of positrons. Further analysis of these data and better statistics from the coming years of TETRA-II observations will lead to a more complete catalog with details of these lightning leader produced events and a better understanding of the production of these bursts of gamma-rays.

References

Abbasi, R. U., et al. Gamma ray showers observed at ground level in coincidence with downward lightning leaders, *Journal of Geophysical Research: Atmospheres*, 123(13), (2018).

Alnussirat, S., et al. Simultaneous space-based observations of terrestrial gamma-ray flashes and lightning optical emissions: investigation of the TGF production mechanisms, *Phys Rev. D*, SUBMITTED, (2019).

Celestin, S., et al. Energy and fluxes of thermal runaway electrons produced by eponential growth of streamers during the stepping of lightning leaders and in transient luminous events, *Journal of Geophysical Research: Space Physics*, 116(A3), (2011).

Chilingarian, A. et al. Ground-based observations of thunderstorm-correlated fluxes of high-energy electrons, gamma rays, and neutrons, *Phys Rev. D*, 82, 043009 (2010).

Chiligarnian, A. et al. Catalog of 2017 thunderstorm ground enhancement (TGE) events observed on Aragats, *Scientific Reports*, (2019).

Connaughton, V., et al. Associations between Fermi Gamma-ray Burst Monitor terrestrial gamma ray flashes and sferics from the World Wide Lightning Location Network, *Journal of Geophysical Research: Space Physics*, 114(A12), (2010).

Dwyer, J. A fundamental limit on electric fields in air, *Geophysical Research Letters*, 30(20) (2003).

Dwyer, J. et al. A ground level gamma-ray burst observed in association with rocket-triggered lightning, *Geophysical Research Letters*, 31(5) (2004a).

Dwyer, J. et al. Measurements of x-ray emission from rocket-triggered lightning, *Geophys. Res. Lett.*, 31 (2004b).

Dwyer, J. X-ray bursts associated with leader steps in cloud-to-ground lightning, *Geophysical Research Letters*, 32(1) (2005).

Dwyer, J. et al. A comparison between Monte Carlo simulations of runaway breakdown and terrestrial gamma ray flash observations. *Geophysical Research Letters*, 32 (2005).

Dwyer, J. Source mechanisms of terrestrial gamma-ray flashes, *Journal of Geophysical Research*, 113 (2008).

Dwyer, J. The relativistic feedback discharge model of terrestrial gamma-ray flashes, *Journal of Geophysical Research: Space Physics*, 117(A2) (2012).

Dwyer, J. et al. Observation of a gamma-ray flash at ground level in association with a cloud-to-ground lightning stroke, *Journal of Geophysical Research*, 117 (2012).

Enoto, T. et al. Photonuclear reactions triggered by lightning discharge, *Nature*, (2017).

Fishman, G. J., et al. Discovery of intense gamma-ray flashes of atmospheric origin, *Science*, 264(5163), 1313-1316 (1994).

Goodman, S. J. The goes-r geostationary lightning mapper (glm), *Atmospheric research*, 125, 34 (2013).

Grefenstette, B. W. et al. First RHESSI terrestrial gamma ray flash catalog, *Journal of Geophysical Research: Space Physics*, 114(A2), (2009).

Grove, J. E. et al. A four-year survey of terrestrial gamma-ray flashes with Fermi LAT, *2012 Fermi Symposium*, (2012).

Gurevich, A., et al. Runaway electron mechanism of air breakdown and preconditioning during a thunderstorm, *Physics Letters A*, 165(5), (1992).

Mallick, S. et al. A study of Xray emissions from thunderstorms with emphasis on subsequent strokes in natural lightning, *Journal of Geophysical Research: Atmospheres*, 117 (2012).

Marisaldi, M., et al. Detection of terrestrial gamma ray flashes up to 40 MeV by the AGILE satellite, *Journal of Geophysical Research: Space Physics*, 115(A3), (2010).

Moore, C. B., et al. Energetic radiation associated with lightning stepped-leaders, *Geophysical Research Letters*, 28, (2001).

NIST XCOM Photon Cross Section Database, https://www.nist.gov/pml/xcom-photon-cross-sections-database, 2018.

Østgaard, N., et al. First half year TGF observations by ASIM, *AGU Fall Meeting*, (2018).

Panasyuk, M., et al. RELEC mission: Relativistic electron precipitation and TLE study on-board small spacecraft, *Advances in Space Research*, 57(3), 835-849, (2016).

Rakov, V., Uman, M. Lightning: physics and effects, *Cambridge Univ. Press, New York*, (2003).

Ringuette, R. et al. TETRA observations of gamma-rays at ground level associated with nearby thunderstorms, *Journal of Geophysical Research: Space Physics*, 118(12), 7841-7849 (2013).

Roberts, O. J., et al. The first Fermi-GBM terrestrial gamma ray flash catalog, *Journal of Geophysical Research: Space Physics*, 123(5), (2018).

Roussel-Dupre, R., Gurevich, A. On runaway breakdown and upward propogating discharges, *Journal of Geophysical Research: Space Physics*, 101(A2), (1996).

Smith, D. et al. The RHESSI spectrometer, *The Reuven Ramaty High-Energy Solar Spectroscopic Imager (RHESSI)*, 33-60, Springer, (2003).

Smith, D. et al. The rarity of terrestrial gamma-ray flashes, *Geophysical Research Letters*, 38(8), (2011).

Tran, M. et al. A terrestrial gamma-ray flash recorded at the lightning observatory in Gainesville, Florida, *Journal of Atmospherics and Solar-Terrestrial Physics*, 136, 86-93 (2015).

Ursi, A. et al. Terrestrial gamma-ray flashes in the BeppoSAX data archive, *Journal of Atmospheric and Solar-Terrestrial Physics*, 156, (2017).

Xu, W. et al. Source altitudes of terrestrial gamma-ray flashes produced by lightning leaders, *Geophysical Research Letters*, 39(8), (2012).

Appendix A. Electronics

Each box is divided into two devices each containing its own front end board to handle up to 10 incoming signals and its own National Instruments card. Figure A.1 shows the circuit diagram for a channel connected to a single PMT on a front end board. The signal from the PMT comes in and is split into two separate signals, a fast digital and a slower analog pulse. The digital signal is sent directly to the FPGA board that handles the logic for the triggering algorithm. If two PMTs viewing a single BGO detect an event in coincidence, or a PPS from the GPS antenna arrives, a trigger signal is generated. The initially negative PMT pulse is amplified and fed to a sample-and-hold circuit (hold time 13μs). This peak and hold gives the National Instruments analog-to-digital (ADC) converter, with a 1 Msample / s readout speed, enough time to probe the maximum height of all 10 channels on the front end board. The analog pulse is then zeroed in time for the next event.

There is a single GPS board and antenna system installed in each box. This board sends a GPGGA string directly to the computer board to initalize the software and name the data file. The GPGGA string contains information such as UTC time, latitude, longitude, and strength of GPS lock. From the GPS board, 2 different signals are output each second. One is a negative $\sim$1.5 V with a 400 ns duration. This signal is sent directly to the front end board and then to the FPGA for triggering. The second is a postive $\sim$1.5 V pulse lasting $\sim$2 μs that is sent to the GPS channel on the front end board. This is the only unique channel on the board, as the other 9 are used for PMT signals from detectors. This is the pulse that is probed by the NI ADC and can be used in analysis to locate the position of the PPS in the analog file.

Each box also contains a single Field Programmable Gate Array (FPGA) board that handles the trigger logic for both devices. Input to this board via ribbon cable are the fast digital signals from the PMT front end board channels along with the fast GPS signal sent to the front end board. If any of the 4 possible trigger conditions is met, the GPS PPS or

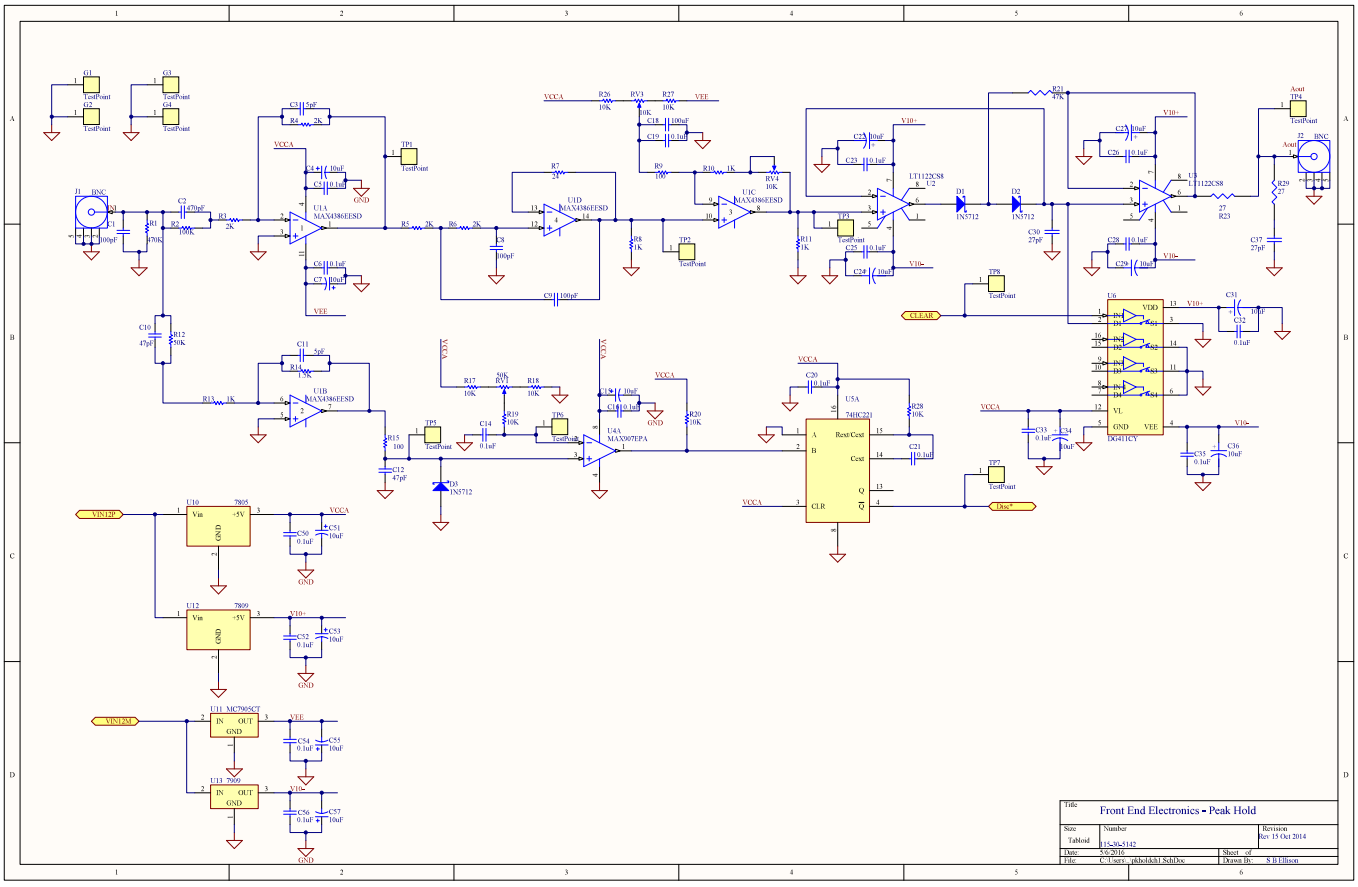

Figure A.1. Diagram of single channel on front end board.

a pair of channels viewing a single BGO, then a signal is sent back to the system to read out the front end channels.

Figure A.2 shows the power layout within a TETRA-II box. Each box is powered from a typical wall outlet (110 V) on each rooftop. A 27 V AC IOTA Power Supply is then used to supply the power to individual components of the box. The full 27 V goes to three components: the high voltage (HV) converter to supply the 1.15 kV to the PMTs, a DC to DC converter to supply $\pm$ 12 V to each front end board the computer power board that connects to the CPU board. This power board powers the CPU board and outputs 5 V to the solid state hard drive and 12 V that is sent to a 5 V regulator to supply the FPGA and GPS boards with 5 V. In addition to the power from the IOTA supply, two 12 V car batteries are connected in series to the power supply. This will provide the needed 24 V when the power from the outlet is cut off during outages.

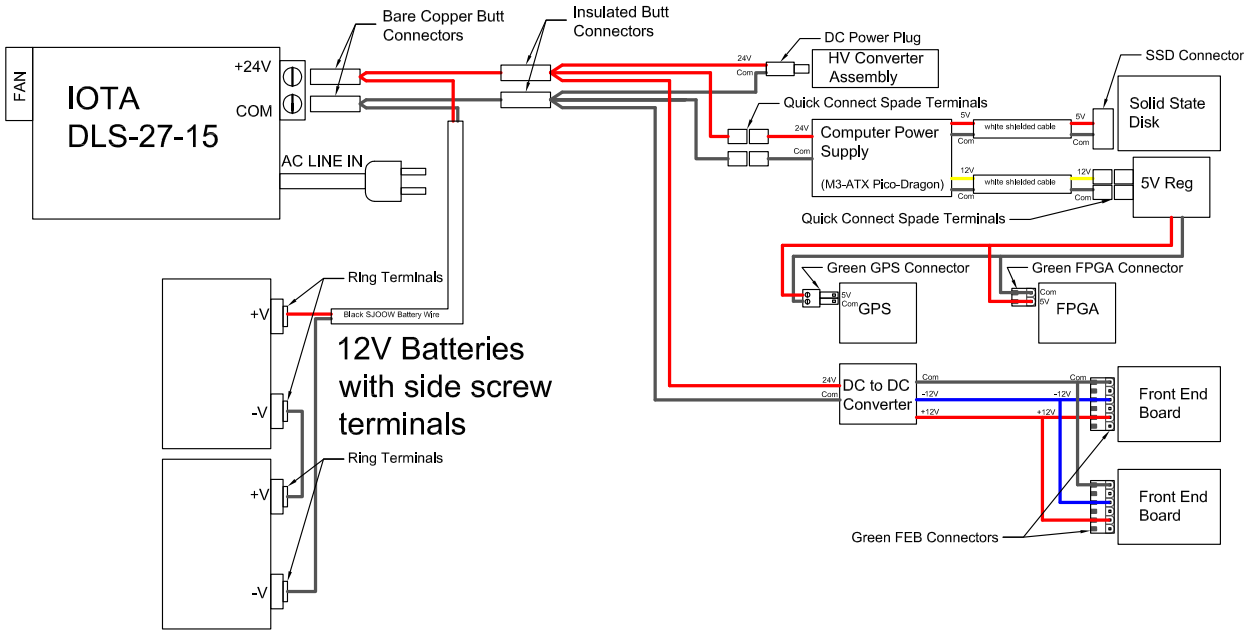

Figure A.2. Power layout in TETRA-II box.

Appendix B. Data Processing

The raw data from the Labview data collection software is stored in tdms files. This allows for Direct Memory Access and faster writing speeds. For each device within a box, four separate files are made: 3 counter files containing timestamp information that will be called counter 1, counter 2, and counter 3, and 1 analog file containing PMT channel information. The Labview software utilizes the 20 MHz clock in the NI card. This clock then counts up from 1 to ∼20,000,000, or 1 "tic" or "count" of the clock every 50 ns. This clock count for each event is the value that is written in each of the counter files.

The counter 1 file contains the master list of timestamp triggers for each of the two devices in the box. Whenever any of the BGO connected to the device are hit and pass the logic of the FPGA board or the PPS from the GPS board comes in the NI clock counter value is recorded. This can only be the case if the system is not currently reading out data from a previous trigger. For example, due to the readout time of each front end channel, if a trigger is seen within 13 μs of a previous trigger the new hit will not be written in the counter 1 file. This file is used as a master list for the set of files since it contains the counter values for all 4 of the conditions that can trigger the system (3 BGO PMT coincidences plus one GPS PPS per device). Regardless of which of the 4 trigger conditions is met, when this timestamp is written to the counter 1 file, the analog file is also written. The analog file contains the ADC channel for the observed peak height seen by every channel on the front end board. This means that no matter which of the BGO and PPS trigger the system, the voltage is read and converted to a channel for every PMT and the GPS for the given device.

The counter 2 file and the counter 3 file both behave in the same way, but for separate BGO, which we will call BGO 2 and BGO 3 respectively. For the counter 2 file, any time that BGO 2 is hit with both of its PMTs seeing a signal that passes the logic of the FPGA board, a "counter" value is written. In this case, the counter 2 file will only have timestamps associated with a single BGO, but it is no longer restricted by the readout time

of the entire system. A pure, un-gated set of timestamps will be obtained for this BGO, even if ADC values for each of these times will not be recorded. This process behaves the same way for the counter 3 file and BGO 3.

To process the raw data and convert the "counter" values recorded to timestamps, a Python script was written that runs once a day looping through the day's files. First, the counter 1 file is read in to find the PPS positions and values. Searching this file for 2 counter values that are approximately 20,000,000 apart gives confidence that the PPS is found. Typically, counter values that are ∼19,500,000 apart are found 600 times within a single counter 1 file. These are the 600 seconds present within the 10 minute file. On average, the difference between the number of "counts" between any 2 PPS will not vary by more than 1 throughout an entire 10 minute file. With the number of "counts" known for a given second, this can be used to convert each "counter" value in a counter file to a fraction of the second. Using this fraction, the GPGGA string with the timestamp of the start of the file, and the number of PPS that have passed within the file, a timestamp can be derived from any "counter" value.

With the clock information from the counter 1 file, the "counters" in the remaining counter files can be converted to timestamps in the same way. Now with three sets of timestamps, a unique set of timestamps can be collected across all 3 BGO and the ADC values from the analog file can be read in directly. This set of data is then written to an hdf5 file to be read in and analyzed searching for events. A file spacer of -40000 is placed at the end of each 10 minute file in both the list of times and the list of ADCs to assist and confirm alignment in post-processing analysis. These full day files allow for the day's data to be histogrammed searching for bursts and extended duration increases in rate as well as for extended background spectra. Once timestamps of interest for event candidates are determined, the hdf5 files and the individual tdms file of interest can be further examined for specific energy information.

Vita

Donald John (DJ) Pleshinger was born in Cleveland, Ohio in May 1991. He was raised in Dover, OH and graduated from Dover High School in 2009. In 2009 DJ began attending Ohio Northern University where he earned a bachelor of science majoring in physics and applied mathematics with a minor in astronomy in 2013. DJ then moved to Baton Rouge, LA to attend Louisiana State University to pursue his Doctor of Philosophy in physics under the supervision of Dr. Michael L. Cherry.